Miner Deposita (2007) 42:145–173
DOI 10.1007/s00126-006-0098-y

ARTICLE

Gold ore-forming fluids of the Tanami region, Northern Australia

Terrence P. Mernagh · Andrew S. Wygralak

Received: 1 January 2006 / Accepted: 5 September 2006 / Published online: 7 December 2006

Abstract Fluid inclusion studies have been carried out on major gold deposits and prospects in the Tanami region to determine the compositions of the associated fluids and the processes responsible for gold mineralization. Pre-ore, milky quartz veins contain only two-phase aqueous inclusions with salinities ≤19 wt% NaCl eq. and homogenization temperatures that range from 110 to 410°C. In contrast, the ore-bearing veins typically contain low to moderate salinity (<14 wt% NaCl eq.), $H_2O+CO_2\pm CH_4\pm N_2$-bearing fluids. The CO_2-bearing inclusions coexist with two-phase aqueous inclusions that exhibit a wider range of salinities (≤21 wt% NaCl eq.). Post-ore quartz and carbonate veins contain mainly two-phase aqueous inclusions, with a last generation of aqueous inclusions being very $CaCl_2$-rich. Salinities range from 7 to 33 wt% NaCl eq. and homogenization temperatures vary from 62 to 312°C. Gold deposits in the Tanami region are hosted by carbonaceous or iron-rich sedimentary rocks and/or mafic rocks. They formed over a range of depths at temperatures from 200 to 430°C. The Groundrush deposit formed at the greatest temperatures and depths (260–430°C and ≤11 km), whereas deposits in the Tanami goldfield formed at the lowest temperatures (≥200°C) and at the shallowest depths (1.5–5.6 km). There is also evidence in the Tanami goldfield for late-stage isothermal mixing with higher salinity (≤21 wt% NaCl eq.) fluids at temperatures between 100 and 200°C. Other deposits (e.g., The Granites, Callie, and Coyote) formed at intermediate depths and at temperatures ranging from 240 to 360°C. All ore fluids contained $CO_2\pm N_2\pm CH_4$, with the more deeply formed deposits being enriched in CH_4 and higher level deposits being enriched in CO_2. Fluids from deposits hosted mainly by sedimentary rocks generally contained appreciable quantities of N_2. The one exception is the Tanami goldfield, where the quartz veins were dominated by aqueous inclusions with rare CO_2-bearing inclusions. Calculated $\delta^{18}O$ values for the ore fluids range from 3.8 to 8.5‰ and the corresponding δD values range from −89 to −37‰. Measured $\delta^{13}C$ values from CO_2 extracted from fluid inclusions ranged from −5.1 to −8.4‰. These data indicate a magmatic or mixed magmatic/metamorphic source for the ore fluids in the Tanami region. Interpretation of the fluid inclusion, alteration, and structural data suggests that mineralization may have occurred via a number of processes. Gold occurs in veins associated with brittle fracturing and other dilational structures, but in the larger deposits, there is also an association with iron-rich rocks or carbonaceous sediments, suggesting that both structural and chemical controls are important. The major mineralization process appears to be boiling/effervescence of a gas-rich fluid, which leads to partitioning of H_2S into the vapor phase resulting in gold precipitation. However, some deposits also show evidence of desulfidation by fluid–rock interaction and/or reduction of the ore-fluid by fluid mixing. These latter processes are generally more prevalent in the higher crustal-level deposits.

Keywords Tanami region · Gold ore · Northern Australia

Editorial handling: D. Huston

T. P. Mernagh (✉)
Geoscience Australia,
GPO Box 378, Canberra 2601, Australia
e-mail: tmernagh@agso.gov.au

A. S. Wygralak
Northern Territory Geological Survey,
GPO Box 2901, Darwin 0801, Australia

Introduction

The Tanami region is the most prospective gold province of the Paleoproterozoic North Australian craton. Since the

inception of modern exploration in 1975, 12.5 Moz Au (~388 t) has been discovered. This region contains more than 60 gold occurrences, which include those in three established goldfields (Dead Bullock Soak, The Granites, and Tanami), the Groundrush deposit, and several significant gold prospects that include Coyote, Crusade, Kookaburra, and Titania (Fig. 1).

Despite its outstanding gold potential, the geology of the Tanami region was, until recently, known only in broad terms, and the nature of gold-bearing ore-fluids was poorly understood. Initial fluid inclusion studies of the Dead Bullock Soak goldfield were conducted on the Callie deposit by Morrison et al. (1994) and Guoyi (1994). Although these early reports were only reconnaissance studies, the microthermometric results obtained by these authors are consistent with those reported in this paper.

A previous study of fluid inclusions from The Granites goldfield (Adams 1997) examined fluid inclusions in three generations of mineralized quartz veins from the Bullakitchie, Shoe, and Quorn deposits, but only secondary inclusions were found. Most inclusions were H_2O-rich with a consistent vapor/liquid ratio, but some solid- or CO_2-bearing inclusions were also present. All inclusions homogenized to the liquid phase over a wide range of temperatures (105–415°C) with a distinct peak between 105–195°C. Salinities ranged up to 39.7 wt% NaCl eq. Depressed eutectic melting temperatures indicated the presence of Na-, K-, Ca-, and Mg-bearing chlorides. Final melting temperatures of CO_2 were close to −56.6°C, indicating that no other gas species was present.

The first fluid inclusion study of the Tanami goldfield was on the Hurricane-Repulse deposit (Tunks 1996). Inclusions in pre-ore quartz veins were reported to have salinities ranging from 15 to 21 wt% NaCl eq. and a mean homogenization temperature of 129°C, whereas inclusions in post-ore calcite veins had salinities ranging from 16 to 22 wt% NaCl eq. and a mean homogenization temperature of 149°C. Inclusions in ore-stage quartz had salinities ≤11 wt% NaCl eq. and a mean homogenization temperature of 217°C. Tunks (1996) noted coexisting liquid- and vapor-rich primary fluid inclusions (but no CO_2-bearing inclusions were reported) in a single ore-stage sample and (assuming an NaCl–H_2O fluid) estimated a depth range of 150–300 m (for hydrostatic conditions) or 50–100 m (for lithostatic conditions). However, he considered such depths to be unrealistically shallow and erroneous due to probable closed system conditions that are unacceptable for this method of calculation.

The aim of this study is to improve our understanding of the fluid chemistry and conditions of mineralization at the major deposits and prospects in the Tanami region. Although some preliminary fluid inclusion data are available, they are typically based on a small number of analyses and are not comprehensive. Furthermore, the range of temperatures and pressure and the apparent scarcity of CO_2 at some deposits have raised important questions about ore genesis. In this study, we report a more comprehensive analysis of fluid inclusions in pre-ore, ore-bearing, and post-ore veins from selected deposits. The new microthermometric data have also been supplemented with laser Raman microprobe analyses and stable isotope studies of selected vein minerals. The results allow a better understanding of the complete fluid history of the Tanami region and allow important questions raised by previous studies, such as the role of CO_2, and the depth of mineralization to be resolved.

Regional geology and structure

Recent extensive studies of the Tanami region (Fig. 1), undertaken by the Northern Territory Geological Survey, are summarized by Crispe et al. (2007).

The Tanami region has undergone a complex tectonic history. Vandenberg et al. (2001) identified at least six regional deformation events. These events include three phases of ductile deformation, the first of which (D_1) is attributed to the Tanami Event that occurred between ~1,840 and ~1,825 Ma. This was followed by a period of volcanism and sedimentation. These newly deposited sequences were then deformed by the D_2 and D_3 deformation events that occurred between ~1,815 and 1,790 Ma. This was accompanied by the intrusion of numerous granitoids (Smith 2000).

The D_4 event involved uplift and erosion of rocks of the Tanami and Ware Groups and unconformable deposition of rocks of the Mount Charles Formation in a locally developed rift. Shear zones, thrust faults, and strike–slip faults attributed to D_5 cut ductile structures throughout the region and postdate the intrusion of regional granitoids and deposition of rocks of the Pargee Sandstone. These D_5 structures are interpreted to control gold mineralization in the Tanami region (Smith et al. 1998; Vandenberg et al. 2001). The last deformation, D_6, and likely additional younger events, involve later thrusting, oblique slip, and normal faulting. Horizontal displacement along associated young structures may reach several kilometers.

Gold mineralization

Gold mineralization in the Tanami region occurs in a number of different stratigraphic units including the Dead Bullock Formation, Killi Killi Formation, and Mount Charles Formation. The majority of gold is hosted by sedimentary rocks, particularly those that were carbona-

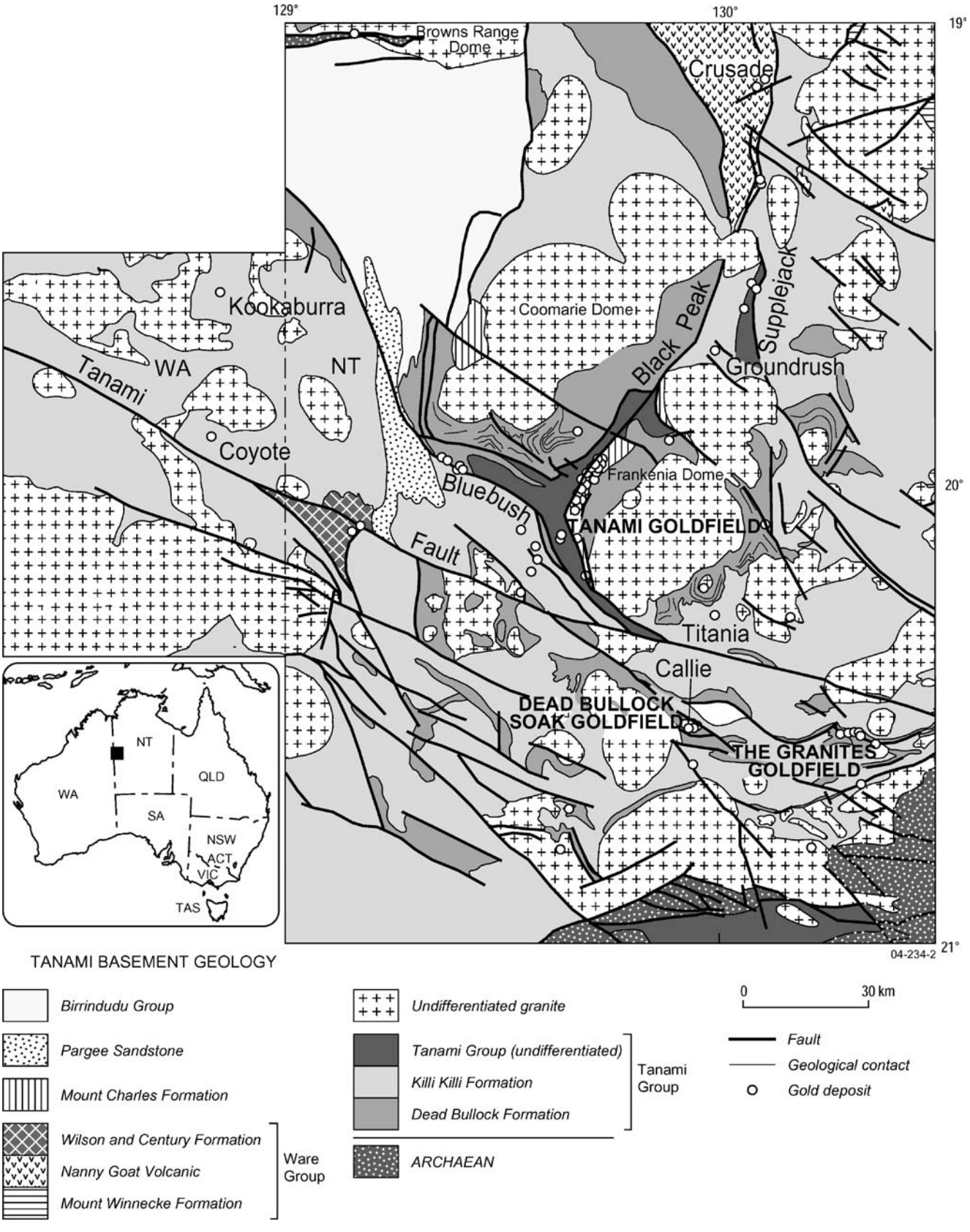

Fig. 1 A simplified basement geology map of the Tanami region showing the locations of the major gold deposits and prospects. Note that the Billabong Complex lies outside the area shown on this map, approximately 50 km southeast of the Granites goldfield

ceous or iron-rich at the time of mineralization. Mafic rocks (e.g., basalt and dolerite) are the other significant host to mineralization.

Deposits hosted mainly by sedimentary rocks

Callie deposit (Dead Bullock Soak goldfield)

The Callie gold deposit is the largest deposit in the Dead Bullock Soak goldfield. The deposit has produced 1.7 Moz (53 t) Au from a total indicated resource of 4.3 Moz (133.7 t) Au (Wygralak et al. 2005). The gold mineralization occurs in the turbiditic units of the Callie member, which is broadly equivalent to the "Upper Blake beds" and "Davidson beds" of Smith et al. (1998). Four stages of veining occur at Callie:

- Pre-mineralization (D_1), bedding-parallel, 5- to 20-mm thick, extensively folded and boudinaged quartz veins consist of patches of relict milky quartz cemented by later recrystallized transparent quartz. Recrystallization may have removed any early generations of fluid inclusions because these veins are generally devoid of inclusions larger than 1–2 μm.
- Syn-mineralization (D_5), auriferous, sheeted quartz veins are composed of subhedral quartz and feldspar (mostly K–feldspar), with accessory epidote, tourmaline, biotite, and amphibole. They form a distinctive set of parallel-sheeted quartz veins, usually 10- to 30-mm thick. These veins may contain visible gold grains that are up to several millimeters in diameter. Veins with visible gold rarely contain sulfides, but minor amounts of pyrite, pyrrhotite, chalcopyrite, arsenopyrite, and marcasite, as well as ilmenite and anatase have been observed (Williams 2007).
- Post-mineralization (D_6) veins consist mostly of quartz, with minor ankerite, pyrite, chalcopyrite, and galena.
- Late post-mineralization (D_{6+}) veins are dominated by ankerite and calcite.

Mineralization at the Callie deposit is controlled by a combination of structural, stratigraphic, and geochemical factors. Mineralization exhibits a strong preference for anticlinal hinges where there is a high-angle intersection between quartz veins and bedding planes. The highest gold grades occur in coarse-grained sedimentary rocks, which have increased porosity and exhibit textural evidence for decarbonization, which is closely associated with mineralization. This has led Huston et al. (2007) to propose a two-stage mechanism for mineralization. The first stage involves initial fluid–rock interaction leading to CO_2 effervescence and gold precipitation near the decarbonization front. The second stage involves remobilization of the gold to enhance the ore-grade of the deposit.

A few pre-mineralization (D_1) quartz veins from Callie were selected for fluid inclusion studies, but most were found to be recrystallized and, hence, did not contain suitable fluid inclusions. Most of the fluid inclusion work at Callie was done on the ore-stage (D_5), sheeted quartz veins and the two generations of post-ore veins. Other deposits of the Dead Bullock Soak goldfield (e.g., Villa, Dead Bullock Ridge, Triumph Hill, Fumarole) are also hosted by rocks of the Dead Bullock Formation, with a strong spatial association with BIF. However, due to time constraints and their relatively less economic significance, these other deposits were not examined in this study.

Coyote deposit

The Coyote gold deposit is intensely sheared, deeply weathered (to 170 m depth), and occurs in a relatively monotonous sequence of fine- to coarse-grained graywacke interbedded with siltstone, rare carbonaceous shale, and mafic intrusive rocks. These rocks are all part of the Killi Killi Formation. It is located near the NW-trending Tanami fault (Fig. 1) and has a total resource of 448,800 oz (14 t) Au (Tanami Gold NL 2005). The open pit is centered on a west-plunging, anticlinal structure, with bedding-parallel mineralization on the limbs of the fold, and patchy but high-grade fold axis-parallel mineralization. Other prospects in this E–W zone, known locally as the "Coyote Mine Sequence," occur ≤7 km from Coyote and a number of other gold anomalies have been identified to the south of Coyote.

Bagas et al. (2007) have recognized up to four generations of quartz veins at Coyote. The earliest quartz veins (with minor chlorite and carbonate) are layer-parallel, non-mineralized, and commonly located in siltstone beds near the contacts with competent sandstone beds. These early veins are cut by both laminated quartz–chlorite veins (with minor pyrite, chalcopyrite, arsenopyrite and rare galena and sphalerite), and planar auriferous quartz veins with patchy biotite, carbonate, arsenopyrite, pyrite, galena, sphalerite, chalcopyrite, bismuth minerals, and free gold.

The mineralized quartz veins occur in an E–W zone for as far as 1 km along strike, to depths of ~200 m (still open at depth). Intersections of as much as 132 g/t Au have been obtained from exploration drilling (Tanami Gold NL 2003), with an estimated average grade of 5.24 g/t Au. The highest gold grades occur near the regolith-to-bedrock transition zone at depths of about 170 m. A late stage of generally planar, buck quartz (white massive quartz, essentially free of accessory minerals) veins cut earlier vein generations and they are usually unmineralized. Only ore-stage quartz veins were examined in this study.

Alteration associated with mineralization is restricted to narrow (<10 mm) chlorite ± sericite ± biotite selvages

adjacent to auriferous veins but the most extensive type of alteration is coarse (≤ 20 mm) arsenopyrite porphyroblasts that are extensively developed in both graywacke and siltstone. There are also more localized alteration assemblages including quartz–sericite–pyrite–chlorite, silica–dolomite (spotting and veining), quartz–K–feldspar, graphite, and chlorite ± biotite. With the exception of the last assemblage, none of these assemblages can be directly correlated with mineralization (Bagas et al. 2007).

Deposits hosted by iron-rich sedimentary rocks

The granites goldfield

The Granites goldfield, located 40 km to the east of the Dead Bullock Soak goldfield, contains four main deposits (Bullakitchie, Shoe, Quorn, and Bunkers Hill) that are hosted by iron-rich sedimentary rocks of the Dead Bullock Formation. Total production from The Granites goldfield was 1.1 Moz (34.2 t) Au (6.4 Mt at 5.5 g/t Au) with a remaining resource of 229,000 oz (7.1 t) Au (Wygralak et al. 2005).

In The Granites goldfield, the sedimentary rocks of the Dead Bullock Formation have been divided into three units, locally known as the Footwall Sequence, the Hangingwall Sequence, and the Main Host Unit. The Footwall Sequence is dominated by interbedded pelitic and psammitic schists, which are metasedimentary rocks composed of quartz, biotite, andalusite, cordierite, almandine, amphibole, and magnetite. The Hangingwall Sequence is dominated by banded pelitic schist grading upwards to psammitic schist. The distinctive feature of the Hangingwall Sequence is the presence of graphite. The Main Host Unit separates the Footwall and Hangingwall Sequences and consists of thinly laminated BIF beds that are silicate-and sulfide-rich, with minor carbonate- and oxide-rich variants. The Inningarra granite intrudes rocks of the Footwall Sequence and thermal metamorphic effects such as random orientation of andalusite crystals in the metasedimentary rocks are recognizable adjacent to the contact. The Granites granite crops out just to the south of The Granites goldfield.

Mineralized veins in The Granites goldfield are characterized by the occurrence of pyrrhotite, arsenopyrite, and loellingite. Other ore minerals include pyrite, marcasite, magnetite, ilmenite, occasional chalcopyrite, and rare galena. Gold occurs as distinct grains, within arsenopyrite, and less frequently, in pyrrhotite and chalcopyrite. Note that up to 30% of the sulfides may reside in the host rocks (Adams 1997). Sulfides in the host rocks commonly are concentrated along bedding-parallel schistosity, and sulfide abundance is independent of vein distribution. According to Adams (1997), most gold mineralization in The Granites goldfield is associated with D_1 veins and with first generation arsenopyrite. However, Vandenberg et al. (2001) argue that the main phase of shearing, which provided conduits for the mineralizing fluid, occurred during D_5. They state that mineralization formed at the intersection of D_5 shears and favorable BIF horizons of the Main Host Unit. Our observations indicate that gold occurs in D_1, D_3, and D_5 veins (with most gold in D_5 veins), mainly as inclusions in arsenopyrite and loellingite, and more rarely, in pyrrhotite and chalcopyrite. However, the majority of gold occurs in close association with arsenopyrite and loellingite within the host rock, mainly in BIF.

Adams (1997) recognized four types of mineralized veins in The Granites goldfield:

- Calc-silicate veins are the oldest generation of veins. They occur throughout The Granites goldfield, but are most abundant in the Bullakitchie deposit. These veins are concordant, were boudinaged during D_1, and are cut by all other vein generations. The veins are 10- to 40-mm thick and are composed of an inner zone of clinozoisite, with subsidiary quartz, diopside, and calcite, and an outer zone of diopside, with lesser clinozoisite, grossular, and hornblende.
- Quartz veins occur in thinly laminated BIF beds of the Main Host Unit. The veins range in thickness from 1 mm to 1 m and are composed of milky white to clear quartz. They are associated with D_1, D_3, and D_5 deformation events.
- Quartz–calcite veins also occur in the Main Host Unit. These discontinuous veins vary from 5- to 200-mm thick and were formed during D_1 and D_3.
- Discontinuous calcite veins formed during D_3, range from 5- to 100-mm thick, and locally contain diopside. These are the dominant vein type in the East Bullakitchie deposit.

Veins with fluid inclusions suitable for analysis were only found in the ore-stage quartz veins of the Main Host Unit. Samples for this study were collected from quartz veins at the Bullakitchie, Shoe, and Quorn deposits of The Granites goldfield.

Deposits hosted by mafic igneous rocks

Tanami goldfield

The Tanami goldfield consists of more than 40 deposits grouped in three clusters (Fig. 1), which are separated by thick (>100 m) regolith-filled paleovalleys. The Tanami goldfield has produced 902,291 oz (28 t) Au and has a remaining resource of 737,666 oz (22.9 t) Au that is distributed among numerous small orebodies, which are considered uneconomic at this stage (Wygralak et al. 2005). The majority of the gold mineralization is hosted in basalt, with the remainder being hosted in turbiditic sedimentary

rocks, both of which belong to the Mount Charles Formation. Locally, the Mount Charles Formation is divided into the Mine, Footwall, and Hangingwall Sequences. The Mine Sequence comprises interbedded basalt, graywacke, mudstone, and shale. The Footwall Sequence is a package of basalt and metasedimentary rocks that is 430 m thick. The Hangingwall Sequence commences with an 85- to 130-m thick basaltic unit overlain by 180 m of interbedded basalt, graywacke, and shale. The entire succession is cut by abundant 1- to 3-m thick felsic dikes and less common mafic dikes.

Tunks (1996) distinguished five generations of veins in the northern part of the Tanami goldfield:

- Pre-ore, dolomite + hematite + sericite ± quartz veins filling small-scale extensional zones along faults in carbonaceous mudstone. These (D_4) veins are <1 mm thick, ≤50 mm long, and do not exhibit alteration haloes.
- Ore-stage (D_5) veins and breccias hosting economic gold mineralization. Two types are distinguished: (1) gray quartz ± sericite ± pyrite veins with chlorite, arsenopyrite, sphalerite, and gold (the gold occurs mainly as inclusions in pyrite), and (2) ankerite + quartz ± chalcopyrite ± chlorite ± gold ± sericite ± chlorite ± calcite (gold occurs mainly as inclusions in chalcopyrite). These discrete veins crosscut or occur in the center of the quartz–sericite–pyrite veins. Both sets of mineralized veins strike in three directions (350–010°, 020–040°, and 060–080°), are controlled by D_5 faults, and dip 65–75° to the east.
- Post-ore (D_6) veins associated with bedding-parallel reverse faults in sedimentary rocks. They are composed of quartz ± pyrite ± chalcopyrite ± covellite in quartz-rich sedimentary rocks, and dolomite ± chlorite ± quartz ± sericite ± hematite in carbonaceous mudstones.
- Post-ore, irregular, 0.1- to 20-mm thick (D_6) veins and stockworks of chlorite ± calcite + ankerite. Some vugs in ankerite are filled with chalcedony.
- Calcite ± chalcopyrite ± quartz (D_6) veins, which are 0.2- to 30-mm thick. These veins are predominately calcite, and they crosscut and displace ore-stage veins.

Quartz-rich, pre-ore veins from the Carbine and Southern pits of the Tanami goldfield were sampled for fluid inclusion and isotopic studies. Both the quartz + sericite and the ankerite + quartz, ore-bearing (D_5) veins from the Carbine, Southern, Legs, Bastille, Redback, Dogbolter, and Jims Main pits were collected for fluid inclusion analysis. Despite a thorough investigation of available post-ore (D_6) carbonate veins from the Tanami goldfield, we failed to find any post-ore veins with fluid inclusions suitable for further study.

Groundrush deposit

The Groundrush deposit is located 100 km north–northwest of The Granites goldfield and has a total resource of 730,000 oz (22.7 t) Au (Wygralak et al. 2005). The orebody is almost entirely hosted by a 90- to 160-m thick, foliated dolerite sill that intrudes metagraywacke of the Killi Killi Formation, and is also <2 km from the inferred margin of the Frankenia Dome (Fig. 1). Structural relations are poorly understood. Mineralized lodes are 10- to 30-m wide and form lenticular anastomosing zones of north-to northeast-trending quartz veins that dip 70–80° to the west. The quartz veins are typically <10 cm wide and contain minor pyrite, arsenopyrite, pyrrhotite, chalcopyrite, and K–feldspar. Gold in the veins occurs as free grains or is associated with arsenopyrite, and to a lesser extent, with pyrite and pyrrhotite. The orebody has gold grades of 3–10 g/t and is open at depth. Mineralization continues over a strike length of 1.1 km, with intersections in drillholes to 140 m below surface. Subtle alteration around mineralized veins consists of chlorite ± carbonate ± actinolite ± biotite. No pre- or post-ore veining has been reported from the Groundrush deposit and all fluid inclusion studies were done on the ore-stage quartz veins.

Analytical methods

Microthermometric data were obtained using a Linkam MDS 600® heating–freezing stage. The Linkam stage was calibrated with a series of synthetic fluid inclusions of known composition. A heating rate of 1°C/min was used to record phase changes below 30°C, whereas a heating rate of 5°C/min was used for phase changes above this temperature. Hence, low temperature phase changes are accurate to ±0.2°C, whereas temperatures above 30°C have an estimated accuracy of ±2°C. Salinity, mole fractions, and bulk density of each inclusion were calculated from equations of state provided within the MacFlinCor program (Brown and Hagemann 1995). For inclusions containing a mixture of CO_2 and CH_4±N_2, the salinity of the aqueous phase was calculated using the Q2 program of Bakker (1997) and the equation of state from Duan et al. (1996). The method of Thomas and Spooner (1988) was used to calculate the salinity of the aqueous phase of CH_4-bearing inclusions.

Laser Raman spectra of fluid inclusions were recorded on a Dilor® SuperLabram spectrometer, which was equipped with a holographic notch filter, 600 and 1,800 g/mm gratings, and a liquid nitrogen-cooled, 2,000×450 pixel, closed circuit diode detector. The inclusions were illuminated with 514.5-nm laser excitation from a Spectra Physics model 2017 argon ion laser, using

5 mW power for the samples, and a single 30-s accumulation. A 100× Olympus microscope objective was used to focus the laser beam and collect the scattered light. The focused laser spot on the samples was approximately 1 μm in diameter. Wave numbers are accurate to ±1 cm^{-1} as determined by plasma and neon emission lines. For the analysis of CO_2, O_2, N_2, H_2S, and CH_4 in the vapor phase, spectra were recorded from 1,000 to 3800 cm^{-1} using a single 20-s integration time per spectrum. The detection limits are dependent upon the instrumental sensitivity, the partial pressure of each gas, and the optical quality of each fluid inclusion. Raman detection limits (Wopenka and Pasteris 1987) are estimated to be about 0.1 mol% for CO_2, O_2, and N_2, and 0.03 mol% for H_2S and CH_4.

Fluid isotopic compositions were calculated using the modal fluid inclusion homogenization temperature and the relevant mineral–fluid fractionations from Clayton et al. (1972, 1989). Stable isotope analyses were carried out at the University of Queensland using standard techniques (Friedman 1953; Clayton and Mayeda 1963). Quartz chips were handpicked and then pulverized in a tema. Powders were reacted overnight at 650°C with BrF_5 in nickel vessels, liberating oxygen that was converted to CO_2 by reaction with an internally heated carbon rod. Direct measurements of $\delta D(H_2O)$ were made by in vacuo crushing of selected samples. Note that with the present techniques, it is difficult to avoid contamination by secondary inclusions. Isotopic analyses were performed with an MM602E mass spectrometer. All isotope data are reported in per mil relative to V-SMOW ($\delta^{18}O$, δD) and PDB ($\delta^{13}C$). Analytical uncertainties are ±0.1‰ for oxygen and carbon and ±2‰ for hydrogen. In some cases, both low- (<300°C) and high-temperature (>300°C) fluid inclusion extractions were carried out to try and distinguish between the aqueous (typically decrepitating at lower temperature) and CO_2-bearing fluid inclusions.

Fluid inclusion petrography

A total of 136 samples were collected from quartz and carbonate veins in diamond drill core, underground exposures, and pit outcrops for textural and petrographic studies (see Appendix for details). From these samples, 52 doubly polished thin sections were made for fluid inclusion studies; the number of fluid inclusions analyzed from each deposit is given in Table 1. At all deposits, the vein and mineral parageneses were carefully determined before commencing the fluid inclusion studies to establish the relative chronology of the trapped fluids. The majority of fluid inclusions in the studied samples were small (<10 μm and typically <5 μm). Growth zones containing primary and pseudosecondary fluid inclusions were observed in some samples, but the majority of samples contained closely packed arrays of inclusions that could not be classified with certainty according to the criteria of Roedder (1984). Data were not collected from inclusions showing signs of leaking or necking-down. Eight different types of inclusions were distinguished (Fig. 2). These are:

- *Type A*. Primary, CO_2-rich inclusions. These may occur along growth zones of quartz crystals as clusters or as single isolated inclusions. At room temperature, they contain a CO_2-rich liquid phase or CO_2-rich liquid + vapor phases. They may also contain small amounts of CH_4 or N_2, and may or may not contain H_2O as an additional phase.
- *Type A-G*. Primary, CO_2-rich inclusions with graphite. These inclusions are similar to Type A inclusions, but also contain variable amounts of graphite, which appears to be an accidentally trapped solid.
- *Type B*. Two-phase, CH_4 (± CO_2) + H_2O inclusions. These inclusions contain 10–30 vol%, CH_4-rich vapor. They may occur as isolated clusters or along healed fractures. Sometimes these inclusions failed to completely freeze during cooling to −196°C and many showed critical behavior during homogenization.
- *Type B-G*. Three-phase, CH_4-bearing inclusions with graphite. These inclusions are similar to Type B, but contained variable amounts of graphite, which appears to be an accidentally trapped solid. Small carbonate crystals were also observed in some of these inclusions.
- *Type C*. Monophase, $CH_4 \pm N_2 \pm CO_2$ vapor inclusions. These inclusions are quite rare and can be distinguished from Type A inclusions by their CH_4- or N_2-rich nature.
- *Type D*. Two-phase aqueous inclusions, which typically contain 5–15 vol% vapor. These inclusions are common in all stages of veining and may be primary or secondary.
- *Type E*. Aqueous inclusions with one or more solid phases. These inclusions typically contain halite and may also contain a vapor phase. They are rare, except in deposits of The Granites goldfield.
- *Type F*. Two-phase brine inclusions. These are generally large, irregular, $CaCl_2$-bearing inclusions with 5–15 vol% vapor. They are secondary inclusions that typically show signs of necking down and generally homogenize at relatively low temperatures.

Results

Microthermometry

To characterize the compositions of the different generations of fluids in the Tanami region, studies of fluid

Table 1 Microthermometric and laser Raman microprobe data for fluid inclusions from selected deposits in the Tanami Region

Inclusion type (number analyzed)	Tm (Car)[a]	Tm (ice)	Tm (clathrate)	X_{CO2} Vap[b]	X_{N2} Vap[b]	X_{CH4} Vap[b]	Wt% NaCl equiv	Th (Total)
Callie Deposit								
Pre-ore veins								
Type D (18)		−0.6 to −10.0 (−4.5)[c]					1.0–14.0 (7.1)	210 to 378 (323)
Ore-bearing veins								
Type A (16)	−58.2 to −56.6 (−56.9)		6.0 to 7.9 (6.3)	0.0–1.0 (0.81)	0.0–0.76 (0.17)	0.0–0.12 (0.02)	3.8–7.3 (6.9)	254 to 326 (311)
Type D (47)		−3.1 to −15 (−11.1)					5.1–20.0 (14.6)	209 to 404 (274)
Post-ore veins								
Type B (29)								400 to 510 (437)
Type D (33)		−4.5 to −14.0 (−10)					7.2–18 (13.9)	111 to 312 (223)
Type F in quartz (9)		−13 to −37 (−26.3)					17.2–33 (26.2)	48 to130 (113)
Type F in carbonate (23)		−8.6 to −21.8 (−19.8)					13.0–26.5 (21.7)	62 to 152 (102)
The Granites Goldfield								
Ore-bearing veins								
Bullakitchie Pit								
Type A (13)	−60.0 to −56.6 (−57.8)		5.9 to 13 (9.0)	0.5–1.0 (0.91)	0.0–0.46 (0.08)	0.0–0.06 (0.01)	0.5–13.5 (5.3)	199 to 312 (271)
Type D (35)		−1.6 to −13.9 (−4.8)					2.5–18.0 (10.3)	116 to 311 (204)
Type E (13)		−19 to −27.4 (−20.8)					22.0–29.0 (25.0)	84 to 175 (131)
Shoe Pit								
Type A (33)	−59.7 to −56.6 (−57.9)		6.0 to 13 (8.7)	0.39–0.97 (0.86)	0.0–0.19 (0.08)	0.0–0.49 (0.06)	1.2–13.5 (4.9)	208 to 305 (266)
Type D (21)		−2.3 to −11.4 (−5.4)					3.7–15.3 (8.1)	121 to 302 (194)
Type E (12)		−19.7 to −23.3 (−19.5)					22.9–24.5 (23.2)	92 to 164 (142)
Quorn Pit								
Type A (28)	−59.3 to −56.6 (−56.9)		6.3 to 12.5 (8.3)	0.15–1.0 (0.67)	0.0–0.73 (0.31)	0.0–0.22 (0.02)	1.9–12.1 (4.2)	201 to 309 (282)
Type D (32)		−1.9 to −13.3 (−5.1)					2.3–16.9 (7.9)	119 to 309 (208)
Type E (11)		−20.1 to −25.3 (−18.9)					23.4–26.7 (21.5)	88–169 (138)
Coyote Prospect								
Ore-bearing veins								
Type A (66)	−62.9 to −56.6 (−58.0)		7.7 to 14.2 (9.4)	0.73–1.0 (0.79)	0.0–0.09 (0.06)	0.0–0.20 (0.07)	0.0–6.7 (2.1)	185 to 408 (308)
Type A-G (14)	−62.4 to −56.6 (−59.2)		4.2 to 11.3 (9.2)	0.74–0.9 (0.84)	0.0–0.08 (0.05)	0.04–0.26 (0.11)	0.0–5.7 (2.4)	
Type B (29)			2.9 to 15.3 (9.9)	0.0–0.18 (0.02)	0.0–0.38 (0.08)	0.62–1.0 (0.90)	0.0–12.5 (2.7)	245 to 389 (325)
Type B-G (9)			7.3 to 11.9 (10.2)	0.0–0.0 (0.0)	0.0–0.15 (0.07)	0.85–1.0 (0.93)	0.0–6.4 (2.5)	
Type C (10)	−59.9 to −56.6 (−57.8)			0.47–0.59 (0.5)	0.3–0.63 (0.39)	0.0–0.24 (0.11)		312 to 417 (359)
Type D (38)		−8.0 to − 0.8 (−3.5)					1.1–11.8(5.5)	183 to 434 (258)
Groundrush Deposit								
Ore-bearing veins								
Type B (47)		−0.7 to −10.0 (−4.9)		0.15–0.87(0.45)	0.0–0.27 (0.03)	0.13–0.85 (0.51)	1.2–13.9 (7.5)	213 to 490 (346)
Type D (18)		−0.1 to −6.9 (−4.5)					0.2–10.4 (6.9)	161 to 277 (207)

Tanami Goldfield								
Pre-Ore Veins								
Southern Pit								
Type D (22)		−0.2 to −15.5 (−6.2)					0.1–19.0 (8.7)	110 to 378 (313)
Carbine Pit								
Type D (25)		−0.6 to −12.2 (−5.4)					0.9–16.1 (7.7)	182 to 410 (277)
Ore-bearing veins								
Southern Pit								
Type A (15)	−56.9 to −56.6 (−56.8)		5.3 to 7.9 (6.4)	0.9–1.0 (0.98)	0.0	0.0–0.1 (0.02)	4.0–11.2 (6.7)	288 to 436 (333)
Type D (46)		−8.8 to −0.2 (−4.4)					0.0–12.0 (6.5)	101 to 375 (216)
Jims Main Pit								
Type A (23)	−56.6		−8.9 to 8.3 (4.9)	1.0	0.0	0.0	2.2–12.7 (8.1)	186 to 358 (289)
Type D (23)		−2.9 to −11.8 (−6.1)					3.1–15.8 (9.0)	192 to 286 (250)
Carbine Pit								
Type D (56)		−3.2 to −18.3 (−10.9)					5.2–21.2 (14.5)	129 to 452 (329)
Legs Pit								
Type D (83)		−0.4 to −6.2 (−3.6)					0.7–9.5 (5.6)	123 to 344 (195)
Bastille								
Type D (46)		−0.1 to −10.9 (−2.1)					0.2–14.9 (3.4)	130 to 391 (194)
Redback								
Type D (25)		−1.2 to −4.2 (−2.4)					2.3–6.4 (3.7)	137 to 351 (205)
Dogbolter								
Type D (33)		0.0 to −14.1 (−3.5)					0.0–17.9 (5.0)	104 to 376 (220)

[a] The carbonic phase may consist of $CO_2 \pm CH_4 \pm N_2$.
[b] Mole fraction of CO_2 or CH_4 in the vapor phase as determined by laser Raman microprobe analysis.
[c] The quoted figures represent the range of the data and the average value is given in parentheses.

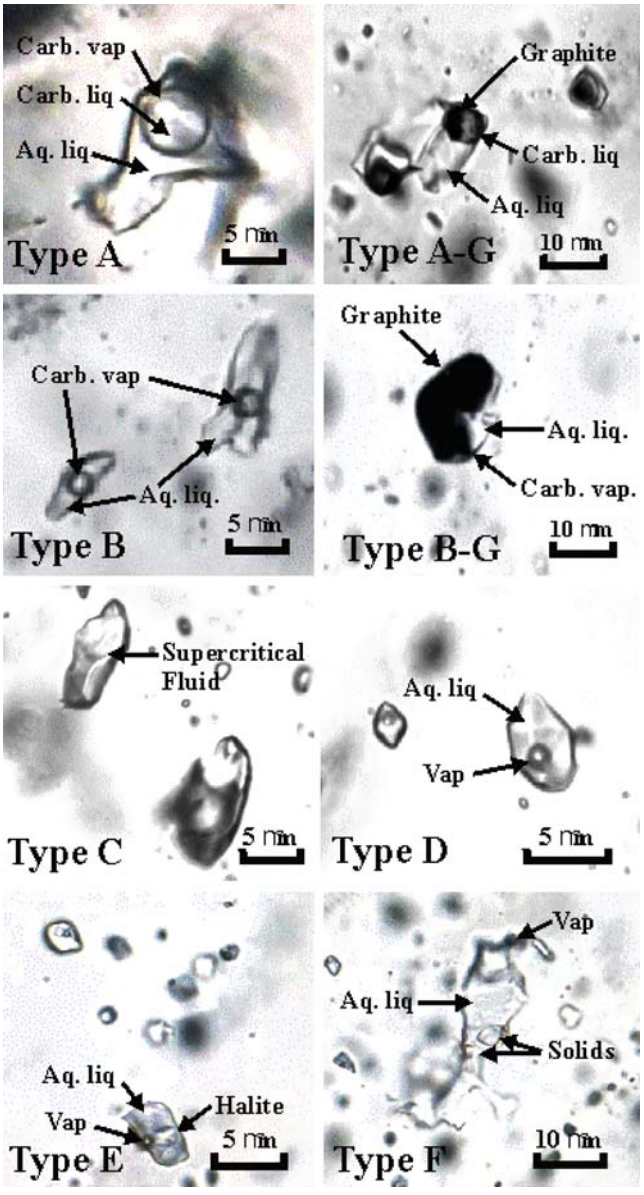

Fig. 2 Photomicrographs of fluid inclusions from the Tanami region. **a** Type A, CO_2-rich inclusions; **b** Type A-G, CO_2-rich inclusions with graphite crystals; **c** Type B, $CH_4 \pm CO_2 + H_2O$ inclusions; **d** Type B-G, CH_4-rich inclusions with graphite crystals; **e** Type C, monophase $CH_4 \pm N_2 \pm CO_2$ inclusions; **f** Type D, two-phase aqueous inclusions; **g** Type E, aqueous inclusions with one or more solid phases; and **h** Type F, two-phase, brine inclusions

inclusions in the pre-ore, ore-bearing, and post-ore veins were carried out where such veins were found to have fluid inclusions suitable for study by microthermometry and/or Raman microprobe spectroscopy.

Due to the small size of the fluid inclusions, only pre- and post-ore veins in drill core were examined from the Callie deposit in the Dead Bullock Soak goldfield and from the Carbine and Southern pits of the Tanami goldfield. Most of the microthermometric data were obtained from ore-stage veins in the Callie deposit, the Bullakitchie, Shoe, and Quorn pits of the Granites goldfield, the Coyote deposit, the Groundrush deposit, and the Southern, Jim's Main, Carbine, Legs, Bastille, Redback, and Dogbolter pits of the Tanami goldfield. All microthermometric and Raman microprobe results are summarized in Table 1.

Pre-ore veins

Callie deposit (Dead Bullock Soak goldfield) The recrystallized, pre-ore, milky quartz veins from the Callie deposit contain rare crystals of transparent quartz with fluid inclusions that were large enough (1–5 μm) for microthermometric work. Only Type D aqueous inclusions were observed. Final ice melting temperatures range from −10 to −0.6°C (Fig. 3a, Table 1), but there is a clear mode at −4°C. The resulting salinities, calculated from the method of Bodnar and Vityk (1994), range from 1 to 14 wt% NaCl eq. These inclusions typically homogenized to the liquid phase, with only a few homogenizing to vapor. They homogenized over the range from 210 to 378°C, although most homogenized at temperatures >280°C (Fig. 4a).

Tanami goldfield The Carbine and Southern pits of the Tanami goldfield contained the only pre-ore quartz veins with fluid inclusions of a suitable size for microthermometry. Only Type D fluid inclusions, as large as 30 μm in diameter, were observed in these veins. These inclusions showed a wide range of ice-melting temperatures from −15.5 to −0.2°C (Fig. 3b). This results in salinities ranging from 0.1 to 19 wt% NaCl eq. (Bodnar and Vityk 1994). The Tm_{ice} histogram has a bimodal distribution with one group of inclusions clustering near −11°C and another group clustering at about −2°C (Fig. 3b). Homogenization temperatures also span a wide range from 110 to 410°C (Fig. 4b). Once again the histogram has a bimodal distribution, with peaks at 280 and 360°C, suggesting that the pre-ore veins may have trapped two generations of fluids. However, it is not possible to identify two spatially distinct populations of fluid inclusions petrographically.

Ore-bearing veins

Callie deposit The ore-bearing veins at Callie contain both Type A and Type D inclusions. Type A, CO_2-rich inclusions, are abundant and have varying degrees of fill ranging from 50 to 100 vol% CO_2. These inclusions were initially cooled to −110°C, with solid CO_2 generally crystallizing between −95 and −105°C. Upon heating, the inclusions showed final CO_2-melting temperatures between −58.2 and −56.6°C. The depression of the melting point to lower values indicates the presence of other gases (CH_4 and N_2), which is in agreement with the Raman microprobe

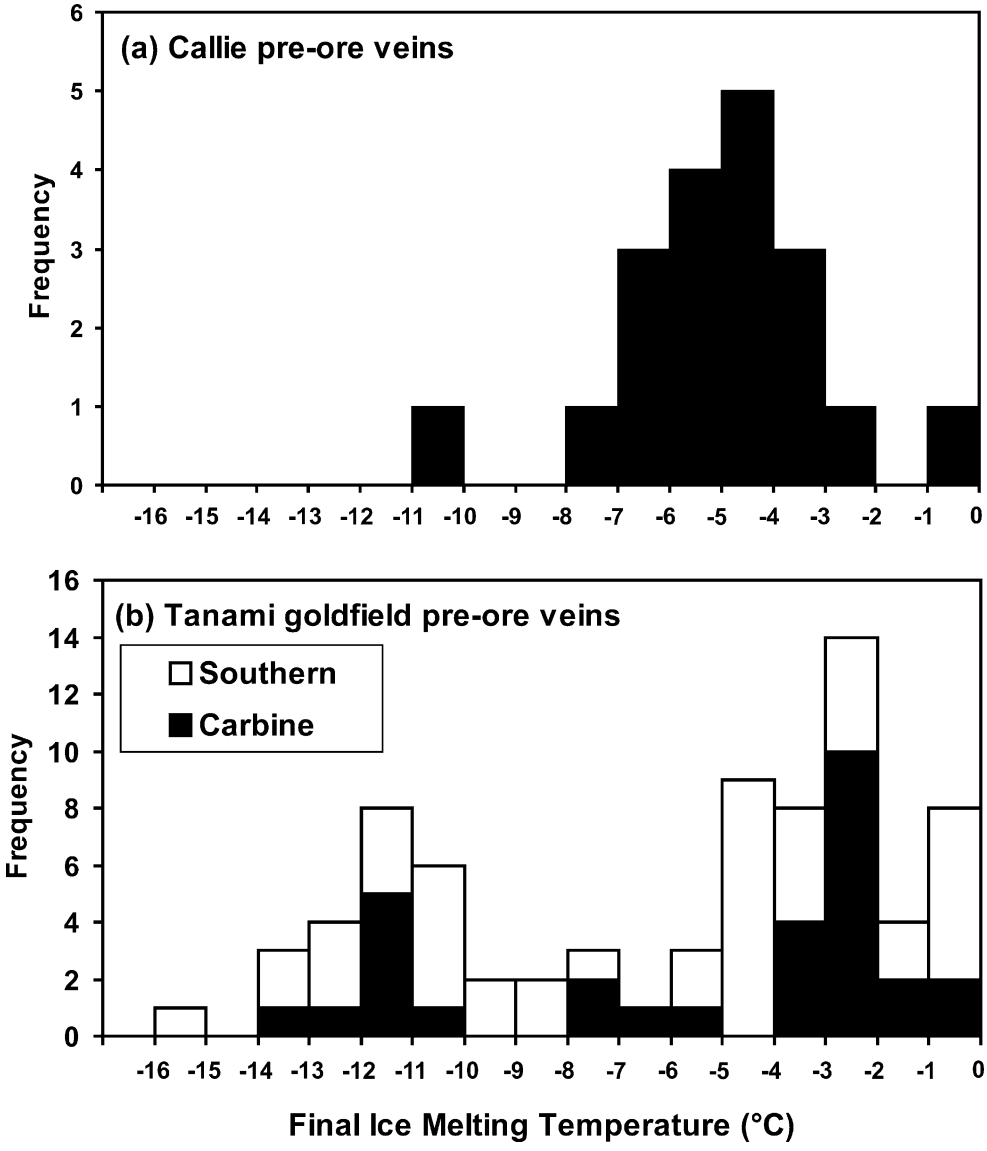

Fig. 3 Histograms showing the final ice melting temperature of fluid inclusions in pre-ore veins from **a** the Callie gold mine, and **b** the Tanami goldfield

analyses (Table 1). Type A inclusions exhibited clathrate melting temperatures between 6.0 and 7.9°C. This equates to salinities between 3.8 and 7.3 wt% NaCl eq. (Fig. 5a). Many Type A inclusions decrepitated before total homogenization, but others homogenized over the range of 254 to 326°C with a mode at 300°C (Fig. 6a).

Type D inclusions showed final ice melting temperatures between −15.0 and −3.1°C, suggesting salinities between 5 and 20 wt% NaCl eq. (Fig. 5a). Multiple peaks and the broad spread of data that are observed in the salinity histogram (Fig. 5a) could be due to the fact that some Type D inclusions have been misclassified. Those with lower salinities may actually contain small amounts of CO_2, which were not detected during the microthermometric analysis. Type D inclusions homogenized from 209 to 404°C, with the majority homogenizing between 260 and 320°C (Fig. 6a). Coexistence of Type A and Type D inclusions within individual fluid inclusion trails suggests that phase separation occurred during vein formation.

The granites goldfield Samples for this study were collected from the Bullakitchie, Shoe, and Quorn open pits. All samples from each pit were taken from mineralized quartz and quartz–calcite veins within the Main Host Unit. As the structure and lithology are the same across all three pits, the fluid inclusion data are considered as a single group.

Inclusions in the mineralized quartz and quartz–calcite veins from all three open pits are characterized by an abundance of CO_2-rich Type A inclusions. A small number of aqueous Type D inclusions coexist with the Type A inclusions, and another population of Type E inclusions containing cubic or tabular daughter minerals occur in separate fracture planes.

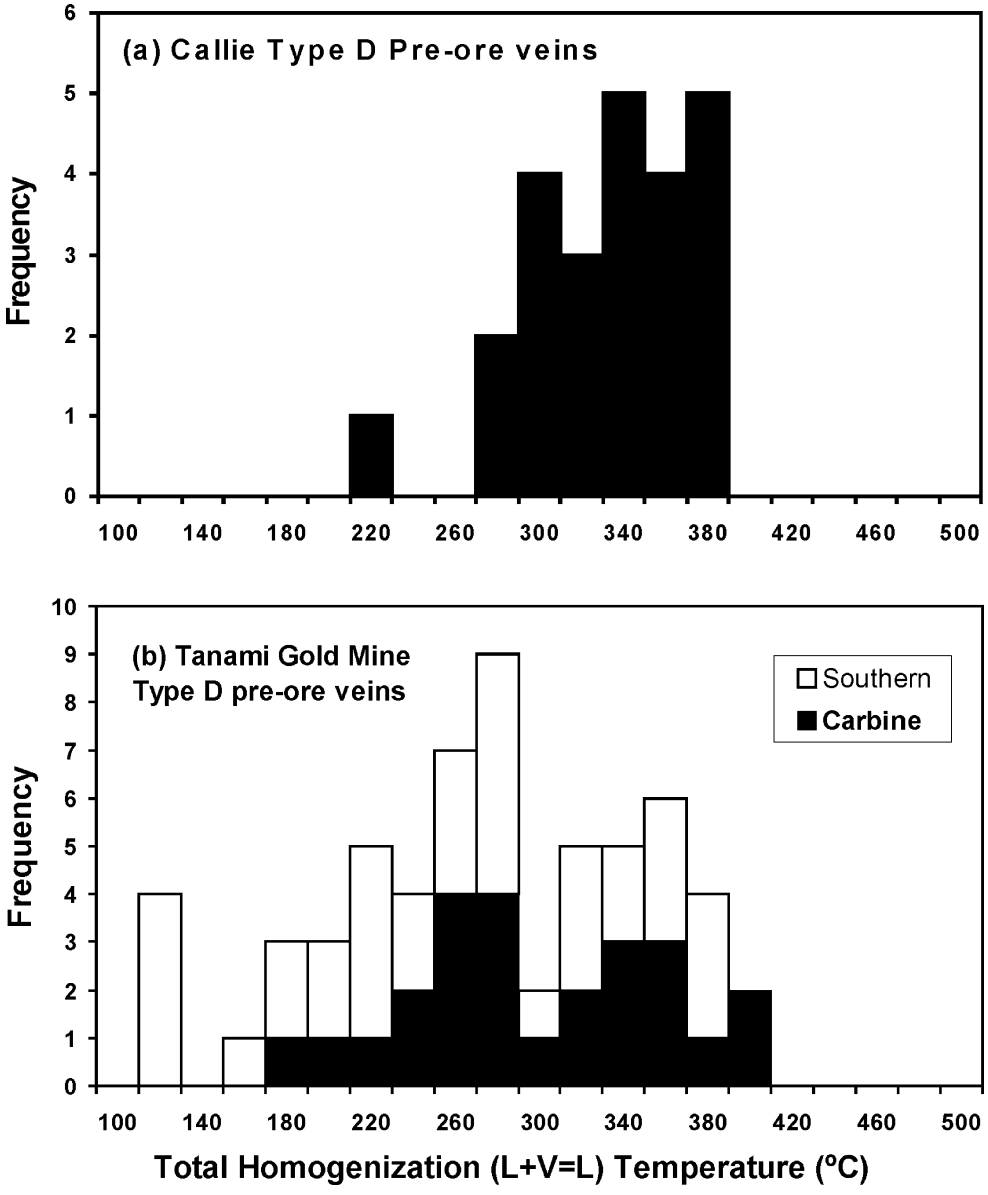

Fig. 4 Homogenization temperatures for fluid inclusions in pre-ore veins from **a** the Callie gold mine, and **b** the Tanami goldfield

Type A inclusions were initially cooled to −110°C with solid CO_2 generally crystallizing between −105 and −95°C. Upon heating, the inclusions showed final CO_2-melting temperatures between −60.0 and −56.6°C. The depression of the melting point to lower values indicates the presence of other gases (CH_4 and N_2), as confirmed by Raman microprobe analyses (Table 1). Clathrate melting temperatures varied from 5.9 to 13.0°C, giving salinities ranging from 0.5 to 13.5 wt% NaCl eq. (Fig. 5b). Type D inclusions showed final ice melting temperatures between −1.6 and −13.9°C, indicating salinities between 2.5 and 18 wt% NaCl eq. Type E inclusions have higher salinities ranging from 22 to 29 wt% NaCl eq. (Fig. 5b).

The carbonic phase of Type A inclusions in samples from all three open pits homogenized from −20.7 to 26.5°C with a mode at 20°C. These homogenization temperatures are in accord with those predicted from the binary CO_2–CH_4 system (Roedder 1984) for mole fractions of CH_4 that are ≤0.5 and agree well with the data from Raman spectroscopy (Table 1). Many of the CO_2-rich Type A inclusions decrepitated before total homogenization, but Type A inclusions that did not decrepitate on heating exhibited total homogenization over the range from 199 to 312°C (Fig. 6b). Type D inclusions homogenized over a similar range from 116 to 311°C. The vapor bubbles in Type E inclusions typically homogenized at relatively low temperatures (Fig. 6b), although some solids did not dissolve at temperatures as high as 550°C (the upper limit of our experiments). This suggests that these solids were either accidentally trapped or that there has been some post-entrapment changes to these inclusions.

Coyote deposit Quartz veins from the Coyote deposit contained closely packed arrays of inclusions that were

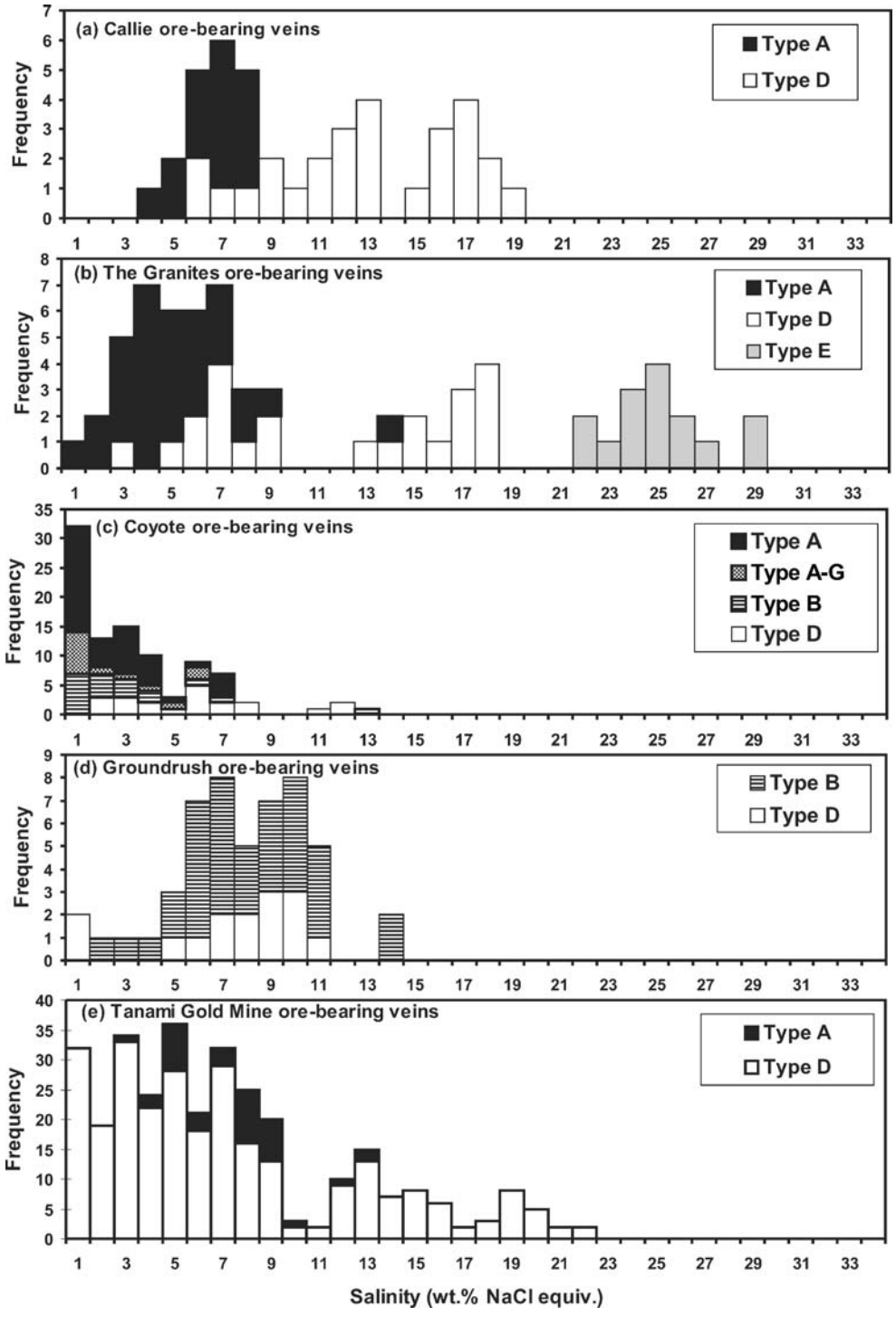

Fig. 5 Histograms of calculated salinities for fluid inclusions from gold-bearing quartz (± minor sulfides) veining in **a** the Callie mine, **b** The Granites goldfield, **c** the Coyote prospect, **d** the Groundrush mine, and **e** the Tanami goldfield

difficult to classify as primary or secondary. Some trails contained a mixture of CO_2 ± graphite-bearing (Type A and A-G) and aqueous Type D inclusions, whereas others contained distinct trails of CH_4 ± graphite-bearing (Type B and B-G) and aqueous Type D inclusions. A few isolated clusters of Type C inclusions, which may be primary, were also observed. Therefore, the quartz veins at Coyote differ from those in the other deposits by having a large number of inclusions with graphite crystals occupying part or nearly all of the inclusions (Fig. 2). The graphite appears to be an accidentally trapped solid because the volume percent varies widely. This suggests that the fluid was carrying particles of graphite and was not totally homogeneous during the growth of the quartz veins.

Type A and type A-G inclusions were initially cooled to −110°C with solid CO_2 generally crystallizing between −105 and −95°C. Upon heating, both graphite-absent and graphite-bearing inclusions showed final CO_2 melting

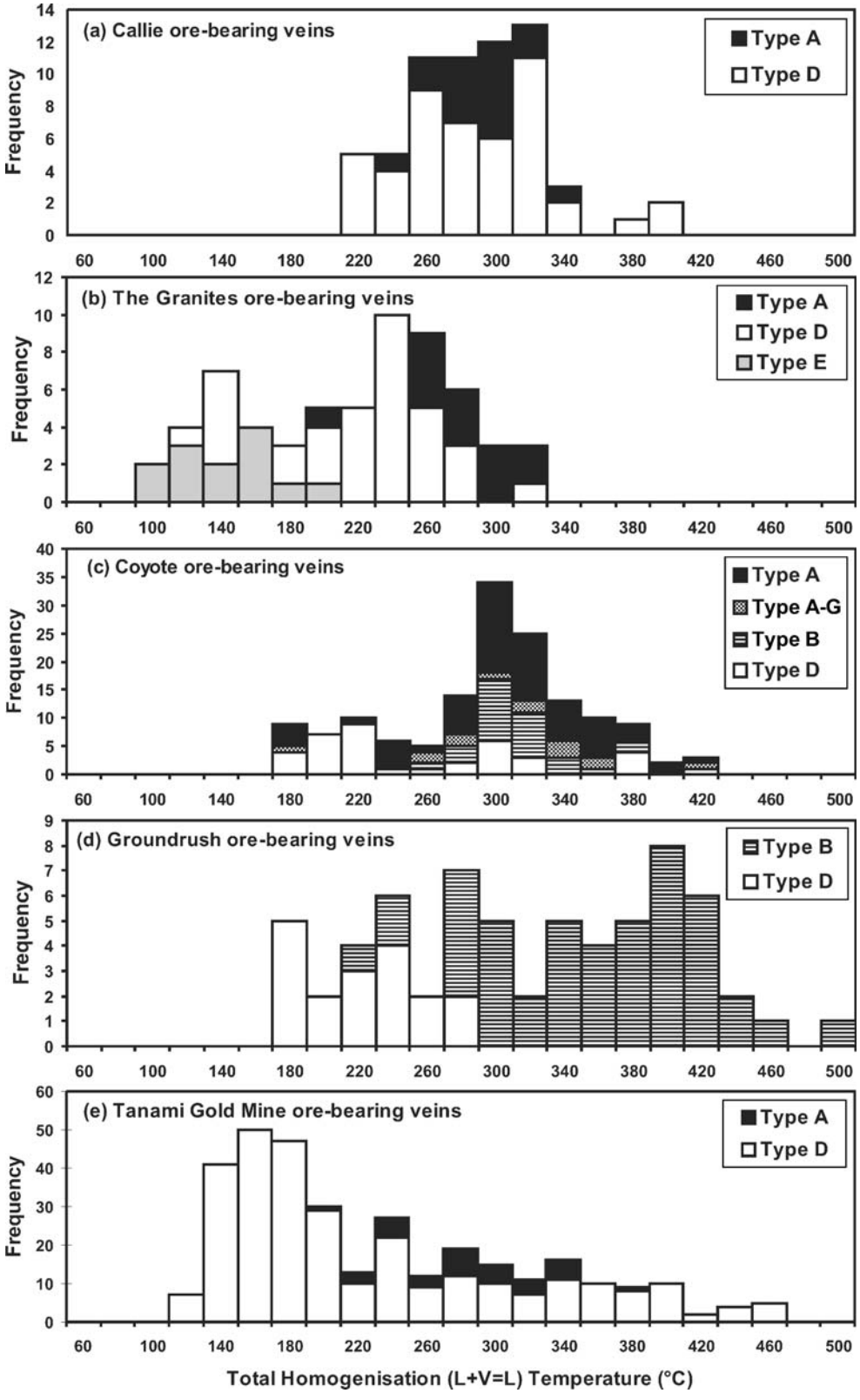

Fig. 6 Histograms of homogenization ($L+V=L$) temperatures for fluid inclusions from ore-bearing veins in **a** the Callie mine, **b** The Granites goldfield, **c** the Coyote prospect, **d** the Groundrush mine, and **e** the Tanami goldfield

temperatures between −62.9 and −56.6°C. The depression of the melting point to lower values indicates the presence of other gases (CH_4 and N_2) in agreement with the Raman microprobe analyses (Table 1). Similar CO_2 melting temperatures are observed in both the graphite-absent and graphite-bearing inclusions. Likewise, similar clathrate melting temperatures were observed in Type A and Type A-G inclusions, and these ranged from 4.2 to

14.2°C (Table 1). As shown in Fig. 5c, salinities for both graphite-absent and graphite-bearing inclusions were generally <10 wt% NaCl eq.

Total homogenization temperatures of Type A and Type A-G inclusions were difficult to obtain as most inclusions decrepitated before total homogenization. Only Type A inclusions completely homogenized to either the liquid or vapor phase. Type A-G inclusions exhibited partial homogenization (i.e., $L + V \rightarrow L$ or $L + V \rightarrow V$), but the graphite particles did not dissolve at temperatures as much as 550°C. The majority of Type A inclusions homogenized to the liquid phase over the range from 290 to 360°C (Fig. 6c).

The aqueous phase of Type B and Type B-G inclusions froze between −40 and −35°C, but no condensation of the vapor phase was observed on cooling to −196°C. These inclusions contain little or no CO_2, and so solid CO_2 is not expected to be observed. However, as the melting temperature of CH_4 is −182.5°C, some liquid CH_4 is expected to condense at the lowest temperatures, but the volume of liquid formed may be too small to detect optically in these inclusions. There are also no observable phase changes near the critical temperature of CH_4 (−82.6°C). Once again, clathrate melting temperatures for both graphite-absent and graphite-bearing inclusions are similar and range from 2.9 to 15.3°C (Table 1). Salinities were <13 wt% NaCl eq., with the mode at 1 wt% NaCl eq. (Fig. 5c). Type B inclusions homogenized to the liquid phase at temperatures from 255 to 389°C with a mode at 310°C (Fig. 6c). This value is in fair agreement with the mode for Type A inclusions above.

The N_2-rich Type C inclusions could not be completely frozen. However, solid CO_2 formed in these inclusions on freezing below −100°C. Upon warming, the vapor bubbles in these inclusions exhibit sublimation of solid CO_2 ($S + V + H_2O \rightarrow V + H_2O$) between −60° and −56.6°C. Depression of the melting point below the triple point of CO_2 (−56.6°C) is due to the presence of N_2 and CH_4.

All aqueous Type D inclusions showed final ice melting temperatures between −8.0 and −0.7°C. This translates to salinities between 1 and 12 wt% NaCl eq. with a mode at 6 wt% NaCl eq. (Fig. 5c). Type D inclusions also homogenized to the liquid phase, but there was a large temperature variation from 180 to 420°C (Fig. 6c). Type D inclusions coexisting with Type A inclusions all homogenize below 250°C with a mode at 220°C, whereas Type D inclusions coexisting with Type B inclusions homogenize above 245°C. The latter group has a mode at 310°C, which coincides with the mode for the Type B inclusions, suggesting that these two groups of inclusions were trapped from a boiling fluid.

Groundrush deposit Type B, CH_4-bearing fluid inclusions are the most abundant inclusions in mineralized quartz veins from the Groundrush deposit. They typically contain 20–30 vol% vapor and occur as isolated inclusions or as short trails, which are crosscut by secondary trails of Type D inclusions. Type B inclusions typically failed to completely freeze during cooling to −196°C; hence, only ice melting temperatures are reported here. These inclusions exhibited eutectic ice melting between −37 and −19°C indicating that NaCl and KCl were the main salts in the aqueous phase. Final ice melting occurred between −10.0 and −0.7, giving salinities ranging from 1.2 to 13.9 wt% NaCl eq. (Fig. 5d). These inclusions homogenized to either liquid or vapor or exhibit critical homogenization. They homogenized from 213 to 490°C, with the majority homogenizing between 260 and 430°C (Fig. 6d).

Secondary Type D inclusions have similar salinities ranging from 0.2 to 10.4 wt% NaCl eq., with the majority having salinities >5 wt% NaCl eq. (Fig. 5d). Homogenization temperatures for Type D inclusions range from 160 to 277°C with a mode at 240°C (Fig. 6d) and all Type D inclusions homogenized to the liquid phase.

Tanami goldfield Very rare Type A, CO_2-bearing inclusions were observed in quartz veins from the Tanami goldfield. The Type A inclusions coexist with Type D inclusions, in growth zones in vuggy quartz from the Southern and Jims Main pits. These inclusions were initially cooled to −110°C, and solid CO_2 generally crystallized between −105 and −95°C. Upon heating, the inclusions showed final CO_2 melting temperatures over a narrow range between −56.9 and −56.6°C. These values indicate that CO_2 and H_2O are the main components of the vapor phase, which is in agreement with the Raman microprobe analyses (Table 1).

The salinity of the aqueous phase of Type A inclusions was generally <10 wt% NaCl eq., but a few values were as saline as 13 wt% NaCl eq. (Fig. 5e). The CO_2-rich phase of Type A inclusions homogenized to the liquid phase over the range of 29.4 to 30.1°C, with the vast majority homogenizing near 30.1°C, which indicates that the density of the carbonic phase was commonly about 0.44 g/cm^3. Total homogenization temperatures ranged from 186 to 436°C, with a mode at 280°C (Fig 6e). The majority of the inclusions homogenized to the liquid phase, with a few of the higher temperature inclusions exhibiting critical behavior.

Type D inclusions, suitable for microthermometry, were found in samples from the Carbine, Southern, Legs, Bastille, Redback, Dogbolter, and Jims Main pits. Salinities for the ore-bearing veins ranged from non-detectable to 21.2 wt% NaCl eq. (Fig. 5c). However, the majority of deposits have salinities <10 wt% NaCl eq. with the exception of the Carbine deposit, which has an average salinity of 14.5 wt% NaCl eq.

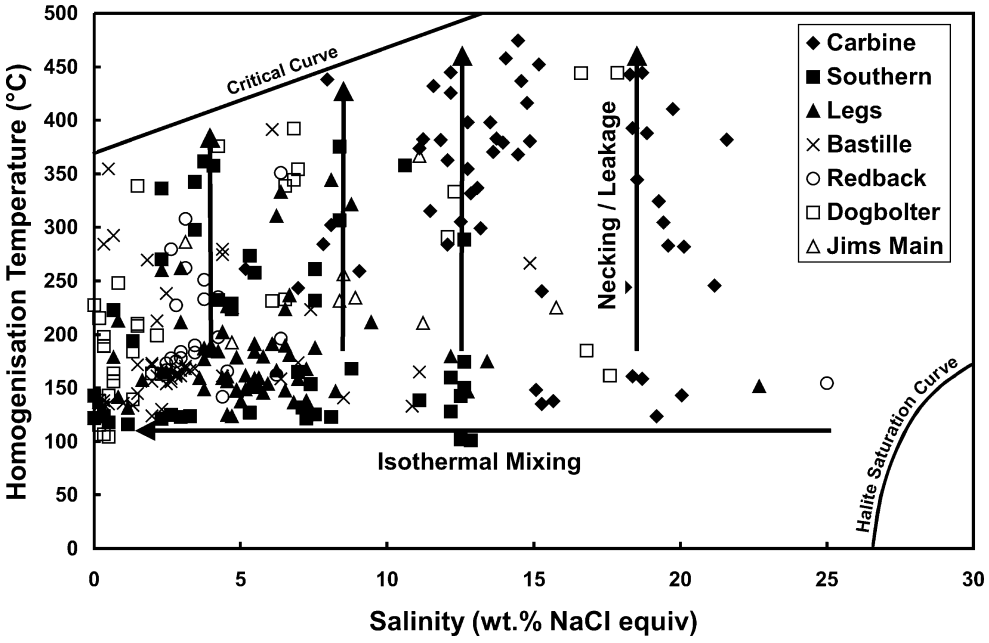

Fig. 7 A plot of salinity vs homogenization temperature for Type D inclusions in ore-bearing veins from the selected pits of the Tanami goldfield. Note that vertical arrays of data (denoted by *vertical arrows*) indicate post-entrapment changes due to either necking down or leakage of the fluid inclusions. The *horizontal arrow* highlights the process of isothermal mixing between a high- and low-salinity fluid (see text for details)

Homogenization temperatures for type D inclusions from ore-bearing, vein quartz in the Tanami goldfield span a wide range from 101 to 452°C (Fig. 6e). There is, however, a clear mode at 170°C, with the data skewed to higher temperatures. This pattern often indicates stretching or leaking of fluid inclusions (Roedder 1984). To further investigate this possibility, the data are displayed on a salinity vs homogenization temperature plot (Fig. 7). Despite the scatter of the data, two effects are apparent. First, post-entrapment changes such as necking or leakage cause elevated homogenization temperatures of some inclusions, as shown by the vertical arrays of data points. However, if these data are ignored, there is strong evidence for an isothermal mixing trend for inclusions homogenizing between 100 and 200°C (Fig. 7). As the homogenization temperatures of the CO_2-rich inclusions are generally higher than 200°C, it appears that both the fluid mixing and the post-entrapment changes occurred after trapping of the CO_2-bearing fluid.

Post-ore veins

Callie deposit Two generations of post-ore veining were observed at the Callie deposit. The earliest post-ore veins (D_6) consist of quartz with minor ankerite, pyrite, chalcopyrite, galena, and sericite, whereas later veins (D_{6+}) are composed of ankerite and/or calcite.

Post-ore D_6 buck quartz veins contain three types of inclusions (cf. Table 1). There is a rare but distinctive population of inclusions with 15–20 vol% vapor (Type B), which did not freeze at temperatures as low as −195°C, and consistently homogenized at very high temperatures between 400 and 510°C. Some of these homogenized either to vapor or by fading of the meniscus. These inclusions concentrate in areas of quartz recrystallization that may have resulted from the intrusion of dolerite sills, although a direct spatial relationship has not been established.

The D_6 veins also contain abundant aqueous Type D inclusions with salinities from 7 to 18 wt% NaCl eq. (Fig. 8a). These inclusions homogenized between 111 and 312°C (Fig. 8b). There are also secondary Type F inclusions that have low homogenization temperatures (48–130°C) and very high salinities of 17.2–33.0 wt% NaCl eq. (Table 1). The presence of $CaCl_2$ in these inclusions is indicated by depression of eutectic melting to temperatures as low as −60°C, together with the brown appearance of the crystals during melting.

Late post-ore, D_{6+} carbonate veins contain a rare population of relatively low temperature inclusions with salinities from 13 to 26.5 wt% NaCl eq. They homogenized from 62 to 152°C with a mode at 100°C.

Tanami goldfield Despite a thorough investigation of available post-ore carbonate veins from the Tanami goldfield, we failed to find any fluid inclusions suitable for further study. However, Tunks (1996) and Tunks and Cooke (2007) reported that aqueous fluid inclusions in post-ore calcite veins had salinities ranging from 16 to 22 wt% NaCl eq. with a mean homogenization temperature of 149°C.

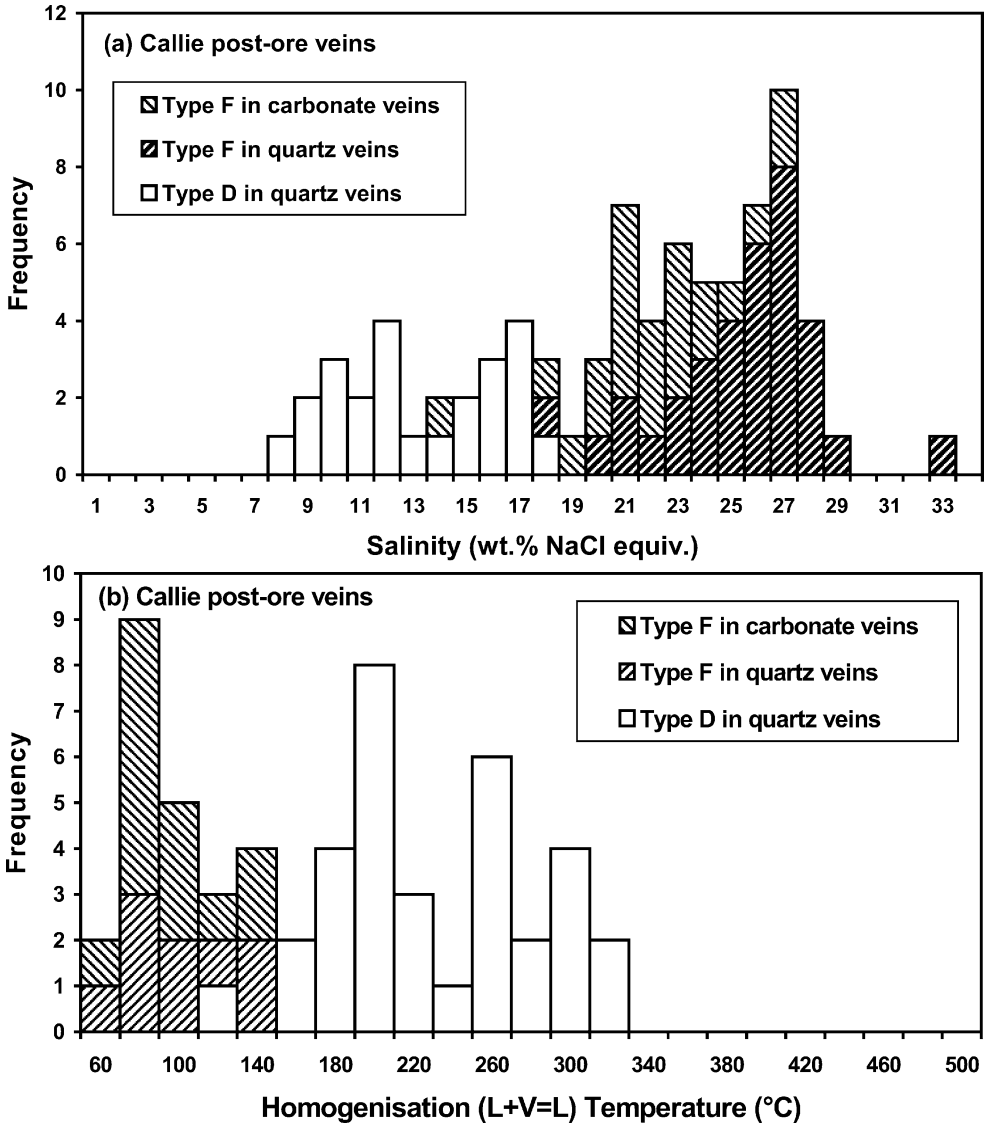

Fig. 8 Histograms of data from fluid inclusions in post-ore veins from the Callie gold mine showing (**a**) salinity of Type D and F inclusions, and (**b**) homogenization ($L+V=L$) temperatures for Type D and F inclusions

Raman spectroscopy

A summary of the laser Raman microprobe analyses of the vapor phase of the fluid inclusions in ore-bearing quartz veins is given in Table 1 and Fig. 9. Raman analysis of Type A inclusions from the Tanami goldfield indicated that the majority of these inclusions contained pure or nearly pure CO_2. A few rare inclusions from the Southern Pit contained as much as 10 mol% CH_4 (Table 1). No gases were detected in the vapor phase of Type D inclusions.

The vapor phase of Type A inclusions from the Callie deposit and The Granites goldfield were of similar composition. The majority of Type A inclusions are CO_2-rich with varying amounts of N_2 and generally minor amounts of CH_4. However, inclusions from The Granites goldfield have higher CH_4 contents (up to 49 mol%) than those from the Callie deposit (up to 12 mol%). No gases were detected in Type D and Type E inclusions from these deposits.

The Raman data from the Coyote deposit can be divided into three distinct groups (i.e., CO_2-rich, CH_4-rich, and a mixed CO_2–N_2 population) on the basis of their gas phase composition (Fig. 9c). The vapor phase of Type A and Type A-G inclusions were generally very CO_2-rich, but may also contain up to 9 mol% N_2 or up to 28 mol% CH_4. Type B and Type B-G inclusions were CH_4-rich with up to 18 mol% CO_2 or up to 38 mol% N_2. Type C inclusions typically contained approximately equal amounts of CO_2 and N_2 with CH_4 contents varying from 0 to 24 mol% (Fig. 9c). The Raman microprobe also confirmed the presence of calcite and disordered carbon (graphite) in Type A-G and Type B-G inclusions. No gases could be detected in the vapor phase of Type D inclusions from this deposit.

The carbonic phase in the majority of inclusions from the Groundrush deposit contained mixtures of CO_2 and CH_4 with little or no N_2. Most inclusions contained almost equal amounts of CO_2 and CH_4 (Fig. 9d), but a few

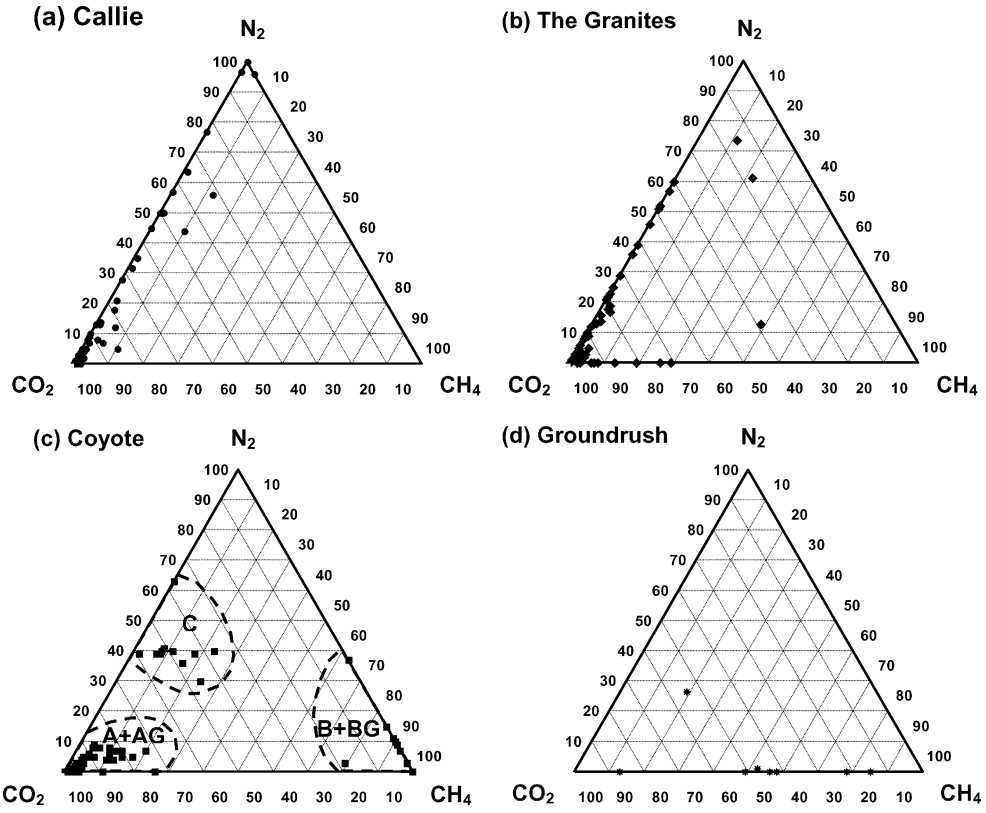

Fig. 9 Plots of CO_2, N_2, and CH_4 concentrations in the carbonic phase of fluid inclusions from **a** the Callie mine, **b** The Granites goldfield, **c** the Coyote deposit, and **d** the Groundrush mine, as determined by laser Raman microprobe analysis. In **c**, the letters *A*, *AG*, *B*, *BG*, and *C* refer to fluid inclusion types (see text for details)

inclusions were either very CO_2-rich or very CH_4-rich. The N_2 contents are generally ≤1 mol%, with only one inclusion exhibiting 27 mol% N_2 (Table 1). No gases could be detected in the vapor phase of Type D inclusions from this deposit.

Overall, the Raman vapor phase data show a variation in gas ratios, with greater amounts of CH_4 in the deeper, higher temperature deposits (e.g., Groundrush) and a higher proportion of $CO_2 \pm N_2$ in higher-level deposits (e.g., Callie and The Granites), with scarce CO_2-rich inclusions in the highest level deposits of the Tanami goldfield.

To determine the major components of the aqueous phase, the laser Raman microprobe was used to identify hydrates that formed in Type D inclusions (from Callie and The Granites goldfield) after freezing them at −180°C (Dubessy et al. 1982). Only the higher salinity fluid inclusions from the ore-bearing veins were analyzed in this study, as these produced larger crystals upon freezing. Hydrates detected using this method include $CaCl_2 \cdot 6H_2O$, $MgCl_2 \cdot 6H_2O$, $MgCl_2 \cdot 12H_2O$.

Isotopic studies

Previously, sulfur isotope studies were carried out at Callie, The Granites, and the Tanami goldfield (Tunks 1996; Adams 1997; Wygralak et al. 2005). These studies found that the ore-related sulfides from the Tanami region generally have a relatively restricted range in $\delta^{34}S$, with most analyses between 4 and 12‰. These values are in accord with either a magmatic or metamorphic source for sulfur in the ore fluids. Valenta (written communication, 1990) and Brincat (1994) carried out preliminary oxygen isotope studies at The Granites gold mine. However, as there have been no comprehensive isotopic studies of the ore fluids from the three major gold mines in the Tanami region, we selected 30 samples from pre-ore, ore-stage, and post-ore veins for oxygen, hydrogen, and carbon isotope analyses. A summary of the stable isotope data from quartz and carbonate samples is presented in Table 2.

Oxygen isotope data

The $\delta^{18}O$ values of pre-ore and ore-stage quartz veins at Callie lie in a narrow range from 12.2 to 12.8‰. The corresponding calculated $\delta^{18}O$ values are 6.2±1.9‰ for fluids in pre-ore quartz veins and 5.5±1.6‰ for fluids in ore-stage quartz veins (Table 2). These values overlap with magmatic and metamorphic water compositions, and indicate that there is little or no meteoric water in ore-stage veins at Callie (Fig. 10). A late-stage incursion of highly evolved meteoric water or basinal brine could account for the shift to lower calculated $\delta^{18}O$ fluid values (1.1±3.8‰).

Ore-stage quartz from The Granites goldfield exhibits a narrow range of $\delta^{18}O$ values from 11.2 to 12.1‰ (Table 2). These data are similar to the range of 10.0–13.1‰ obtained by Valenta (written communication, 1990) and Brincat

Table 2 Summary of stable isotope data for quartz and carbonate samples from the Groundrush, Callie, The Granites, and Tanami gold mines

Goldfield	Stage of veining	Mineral δ^{18}O‰ range, (median)	Trapping temperature[a], °C	Calculated fluid δ^{18}O‰	Inclusion δD‰ range, (median)	Inclusion δ^{13}C‰ range, (median)
Groundrush	Ore quartz (n=1)	11.6	345±80	6.2±2.8	Not analyzed	Not analyzed
Callie	Pre-ore quartz (n=3)	12.2 to 12.8, (12.8)	310±50	6.2±1.9	Insufficient H_2O	−6.6 to −5.8, (−6.2)
Callie	Ore quartz (n=3)	12.7 to 12.8, (12.8)	290±40	5.5±1.6	−85 to −58, (−71)	−7.6 to −5.1, (−5.3)
Callie	Post-ore quartz (n=5)	12.2 to 13.2, (12.8)	200±50	1.1±3.8	−89 to −55, (−72)	−7.2 to −5.1, (−5.9)
Callie	Post-ore siderite (n=2)	12.0 to 13.3, (12.7)	100±50	−12.2±7.2	–	−7.2 to −6.1, (−6.6)
Callie	Post-ore calcite (n=4)	1.6 to 17.8, (11.5)	100	−23.3 to −7.2	–	−11.3 to −4.5, (−7.4)
The Granites	Ore quartz (n=5)	11.2 to 12.1, (11.5)	280±40	3.8±1.8	−71, one only	−8.4 to −7.7, (−8.0)
The Granites	Post-ore quartz (n=1)	9.4	150±50	−5.9±5.6	Insufficient H_2O	Insufficient CO_2
Tanami	Ore quartz (n=6)	15.1 to 19.2, (16.6)	270±50	8.5±2.4	−69 to −37, (−53)[b] −58 to −45, (−51)[c]	Insufficient CO_2
Tanami	Post-ore quartz (n=1)	16.3	150±50	0.8±5.4	−53, −54, two only	Insufficient CO_2

[a] Trapping temperatures are based on fluid inclusion data (see Table 1).
[b] Low temperature extraction
[c] High temperature extraction

(1994). Post-ore quartz from the Shoe deposit has a more ^{18}O-depleted composition of 9.4‰. Calculated fluid δ^{18}O values of ore-stage quartz at 280±40°C are 3.8±1.8‰, which is lower than values typical of unexchanged magmatic or metamorphic fluids. This could be explained by mixing with an evolved meteoric fluid or basinal brine. However, similar depleted oxygen isotope compositions have also been observed in systems involving only magmatic fluids (Higgins 1990), where the effect has been attributed to fractionation between CO_2 and H_2O. Post-ore quartz yielded a calculated fluid δ^{18}O value at 150±50°C of −5.9±5.6‰. The high salinity (see above) and depleted oxygen isotope composition of the post-ore fluid are consistent with highly exchanged meteoric water or high latitude basinal brine.

Vein quartz from the Tanami goldfield is slightly more ^{18}O-enriched and exhibits a wider range of δ^{18}O values than does quartz from the other two goldfields (Table 2). The calculated δ^{18}O value of fluid from ore-stage veins (for a trapping temperature of 270±50°C) is 8.5±2.4‰. These values overlap both the magmatic and metamorphic water fields in Fig. 10. The heavier δ^{18}O values from the Tanami goldfield may also suggest that these deposits have formed at lower temperatures than the other deposits. Some quartz veins in this goldfield have textures indicative of high-level emplacement such as colloform quartz textures and chalcedonic quartz, and both ghost-sphere and radial "flamboyant" textures have been observed in thin sections (Wygralak and Mernagh 2001).

The δ^{18}O values of fluid from a single sample of post ore-stage quartz from the Tanami goldfield is calculated (for a trapping temperature of 150±50°C) to be 0.8± 5.4‰. This relatively light value is consistent with a major influx of meteoric water or high latitude basinal brine.

A single analysis of ore-stage quartz from the Groundrush mine gave a δ^{18}O value of 11.6‰. For an estimated trapping temperature of 345±80°C, this corresponds to a calculated δ^{18}O value of 6.2±2.8‰ for aqueous fluids at Groundrush (Table 2).

Hydrogen isotope data

The hydrogen isotope data are based upon bulk extractions of fluid inclusion waters in quartz. Although care was taken to select samples of quartz with a dominant population of primary fluid inclusions, the complex history of the veins means that they probably contain a mixture of fluid inclusions from different fluids that passed through the veins. This is one factor contributing to the general spread of δD data in Table 2; therefore, some caution needs to be exercised when making interpretations based on these data.

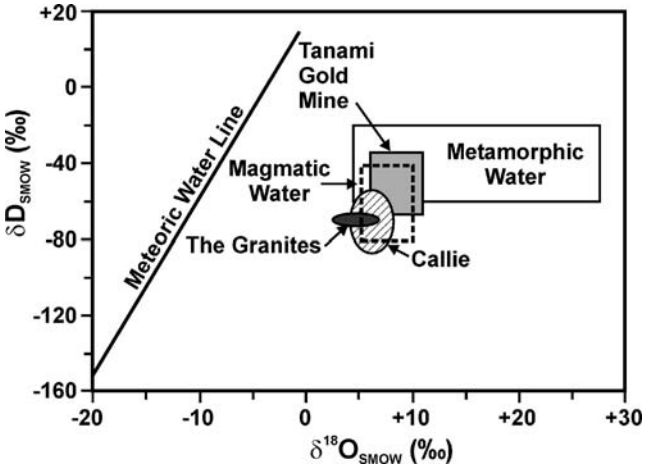

Fig. 10 Calculated oxygen and hydrogen isotopic compositions of mineralizing fluids for deposits from The Granites goldfield, Callie, and the Tanami goldfield. The *solid box* denotes the extent of the metamorphic water field and the *dotted box* denotes the extent of the magmatic water field after Taylor (1987)

Fluid inclusion δD values for ore-stage and post-ore quartz from the Callie deposit exhibit overlapping ranges from −85 to −58‰ and −89 to −55‰ (Table 2). A plot of calculated oxygen and measured hydrogen isotope values shows that the Callie ore fluids are consistent with a fluid of magmatic/metamorphic origin (Fig. 10).

Only one ore-stage quartz sample from The Granites contained sufficient H_2O-rich inclusions for isotopic analysis and had a bulk δD value of −71‰ (Table 2). This measured hydrogen isotope value again suggests a magmatic origin for the ore fluids. However, Adams (1997) suggest a metamorphic origin based on his isotopic data.

Low- (<300°C) and high-temperature (>300°C) fluid inclusion extractions from Tanami goldfield ore-stage quartz were carried out to try and distinguish between the aqueous and CO_2-bearing fluid inclusions, respectively. The data exhibit overlapping δD ranges from −69 to −37 and −58 to −45‰ (Table 2). Post-ore quartz has similar inclusion δD values of −54 and −53‰ for low- and high-temperature extractions, respectively. Figure 10 shows that Tanami ore fluid compositions are consistent with a hybrid magmatic/metamorphic origin.

Carbon isotope data

The CO_2 in fluid inclusions from pre-ore, ore-stage, and post-ore quartz from the Callie deposit exhibit narrow overlapping ranges of δ^{13}C values, with medians of −6.2, −5.3, and −5.9‰, respectively (Table 2). The CO_2 in fluid inclusions in ore-stage quartz from The Granites goldfield exhibits a narrow range of δ^{13}C values from −8.4 to −7.7‰. There was insufficient CO_2 in fluid inclusions in quartz from the Tanami goldfield for carbon isotope analyses. Measured values lie within the range of magmatic carbon that has a δ^{13}C value of −7±2‰ (Hoefs 1980), but they could also result from mixing between organic and marine carbonate. As granitoids and carbonaceous marine sedimentary rocks are both present in the Tanami region, the carbon isotope data are unable to distinguish between a magmatic and an organic source for the carbon in the ore fluids.

Discussion

Trapping conditions of the ore-bearing fluids

The pressure and temperature (PT) at the time the fluid inclusions were trapped can be estimated from the solvus for the appropriate chemical system if it can be shown that the inclusions were undergoing phase separation at the time of trapping. Alternatively, the PT conditions may be estimated from the appropriate isochore(s) if an independent value of pressure or temperature can be obtained for the process that leads to the trapping of the fluid inclusions. These methods have been used to estimate the pressure and the corresponding depth of formation for the deposits considered in this study.

An estimate of the initial composition of the ore-bearing fluid for each deposit is given in Table 3. As there is no available data for the solvus of the H_2O–CO_2–N_2–CH_4–NaCl system, we used the solvus for the system H_2O–10 mol% CO_2–6 wt% NaCl (Schmidt and Bodnar 2000). As both N_2 and CH_4 are nonpolar gases and there is little available data on the H_2O–N_2–CH_4 system, we have used the solvi for the H_2O–CH_4 system as a proxy for the H_2O–N_2–CH_4 system.

At the Callie deposit and The Granites goldfield, the CH_4 content of the inclusions is typically low and the N_2 content is generally less than 20 mol% (Fig. 9). Therefore, the range of pressures estimated from fluid inclusion data for the Callie deposit and The Granites goldfield are represented by the gray shaded region and the hatched region, respectively, in Fig. 11a. For trapping on the solvus, these temperatures translate to pressures between 70 and 130 MPa for the Callie deposit and 80 and 260 MPa for The Granites goldfield. Assuming lithostatic pressures at the time of trapping, this equates to entrapment depths between 2.6 and 5.0 km for Callie and 3.0 to 9.8 km for The Granites goldfield.

At the Coyote deposit, the majority of gas-rich inclusions homogenize between 250 and 370°C, which allows us to define a region in PT space (shown in light gray in Fig. 11b) corresponding to the trapping conditions for these inclusions. This suggests that the mineralized veins could have formed at pressures up to 200 MPa. However, if we take the modes from the microthermometric data as the most probable temperatures of trapping, then mineralization occurred at temperatures of about 290–310°C at pressures

Table 3 Observations from fluid inclusions used to derive original compositions for the ore-bearing fluids

Deposit	Observations supporting homogeneous or heterogeneous trapping	Original homogeneous fluid composition
Callie	Coexisting CO_2-rich, Type A and aqueous, Type D inclusions in individual fluid inclusion trails suggest heterogeneous trapping.	4–7 wt% NaCl eq (based on coexisting Type A and Type D inclusions) 6–16 mol% carbonic phase ($X_{CO2}\leq1.0$, $X_{N2}\leq0.76$, $X_{CH4}\leq0.12$)
The Granites Goldfield	Coexisting CO_2-rich, Type A and aqueous, Type D inclusions in individual fluid inclusion trails suggestheterogeneous trapping.	0–14 wt% NaCl eq (based on coexisting Type A and Type D inclusions) 5–28 mol% carbonic phase ($X_{CO2}\leq1.0$, $X_{N2}\leq0.73$, $X_{CH4}\leq0.49$)
Coyote	Coexisting Type D inclusions with Type A or Type B inclusions in individual fluid inclusion trails suggestheterogeneous trapping.	0–7 wt% NaCl eq (based on coexisting Type A, Type B, and Type D inclusions) 5–30 mol% carbonic phase in Type A ($X_{CO2}\leq1.0$, $X_{N2}\leq0.09$, $X_{CH4}\leq0.26$)
Groundrush	Relatively constant liquid/vapor ratios in primary Type B inclusions (and lack of evidence for heterogeneous trapping) suggest homogeneous trapping or that vapor-rich inclusions were not trapped in these veins.	1–14 wt% NaCl eq 5–25 mol% carbonic phase in Type B ($X_{CO2}\leq0.87$, $X_{N2}\leq0.27$, $X_{CH4}\leq0.85$)
Tanami Goldfield	Primary inclusions in growth zones in quartz from the Southern and Carbine pits contain coexisting 3-phase, CO_2-rich inclusions and two-phase, aqueous inclusions suggest heterogeneous trapping.	2–13 wt% NaCl eq (based on Type A inclusions) 4–10 mol% carbonic phase in Type A ($X_{CO2}\leq1.0$, $X_{CH4}\leq0.1$)

between 90 and 110 MPa (dark gray box in Fig. 11b). This region corresponds to Type A inclusions, with approximately 10 mol% CO_2 and Type B inclusions with about 5 mol% CH_4, and also overlaps with the 220°C constant temperature line in the H_2O+6 wt% NaCl system (the homogenization mode for Type D inclusions coexisting with Type A inclusions). If we assume that the mineralized veins formed at lithostatic pressures, then the highest trapping pressure of 200 MPa gives a maximum formation depth of 7.5 km, but using the modes of 90 to 110 MPa gives a probable formation depth of 3.4–4.2 km.

At the Groundrush deposit, the Raman microprobe analyses of the carbonic phase indicate that the majority of Type B inclusions have approximately equal quantities of CO_2 and CH_4 (Fig. 9). Therefore, the solvi for 50 mol% CO_2 and 50 mol% CH_4 are also shown in Fig. 11c, and the one-phase field lies to the right of these lines. No definite evidence for phase separation could be found in this study (Table 3), and without other geological constraints on the pressures during mineralization, only approximate depths of formation for Groundrush can be estimated.

The gray region in Fig. 11c shows the range of pressures for trapping at temperatures between 260 and 430°C. The isochores between 180 and 252°C for the system H_2O–6 wt % NaCl also pass through the gray region in Fig. 11c. This suggests that the aqueous inclusions at Groundrush may also have been trapped at the time of mineralization and provides an additional constraint on the pressure estimates. Thus, trapping pressures at Groundrush are estimated to be between 150 and 290 MPa, giving formation depths between 5.6 and 11.0 km, assuming lithostatic pressures.

Although quite rare, the CO_2-bearing fluid inclusions are thought to best represent the ore-bearing fluid in the Tanami goldfield (Table 3) for two reasons. First, these are the highest temperature fluids observed in these veins, and thus are most likely to be the initial fluids that entered the veins. Second, as shown in Fig. 7, there have been extensive post-entrapment changes to the aqueous Type D fluid inclusions; they are considered less reliable.

The majority of Type A inclusions from the Tanami goldfield homogenized from 200–340°C; thus, mineralization occurred at pressures between 40 and 150 MPa (gray region in Fig. 11d). Assuming the fluids were initially at lithostatic conditions, the depth of formation is estimated to be between 1.5 and 5.6 km. These values are in good agreement with estimated trapping temperatures of aqueous fluid inclusions from the Hurricane-Repulse pit (Tunks and Cooke 2007). However, it appears likely that the deposits of the Tanami goldfield formed at the shallower end of these estimates, as many of the quartz veins have textures, indicative of high-level emplacement such as colloform quartz textures and chalcedonic quartz, and both ghost-sphere and flamboyant textures have been observed in thin sections (Wygralak and Mernagh 2001).

Mineralization processes

The above data, summarized in Fig. 12 and Table 4, indicate that the gold deposits formed over a wide range of depths from approximately 1.5 to 11 km. Homogenization temperatures for fluid inclusions associated with mineralization range from 200 to 430°C, but there is a general

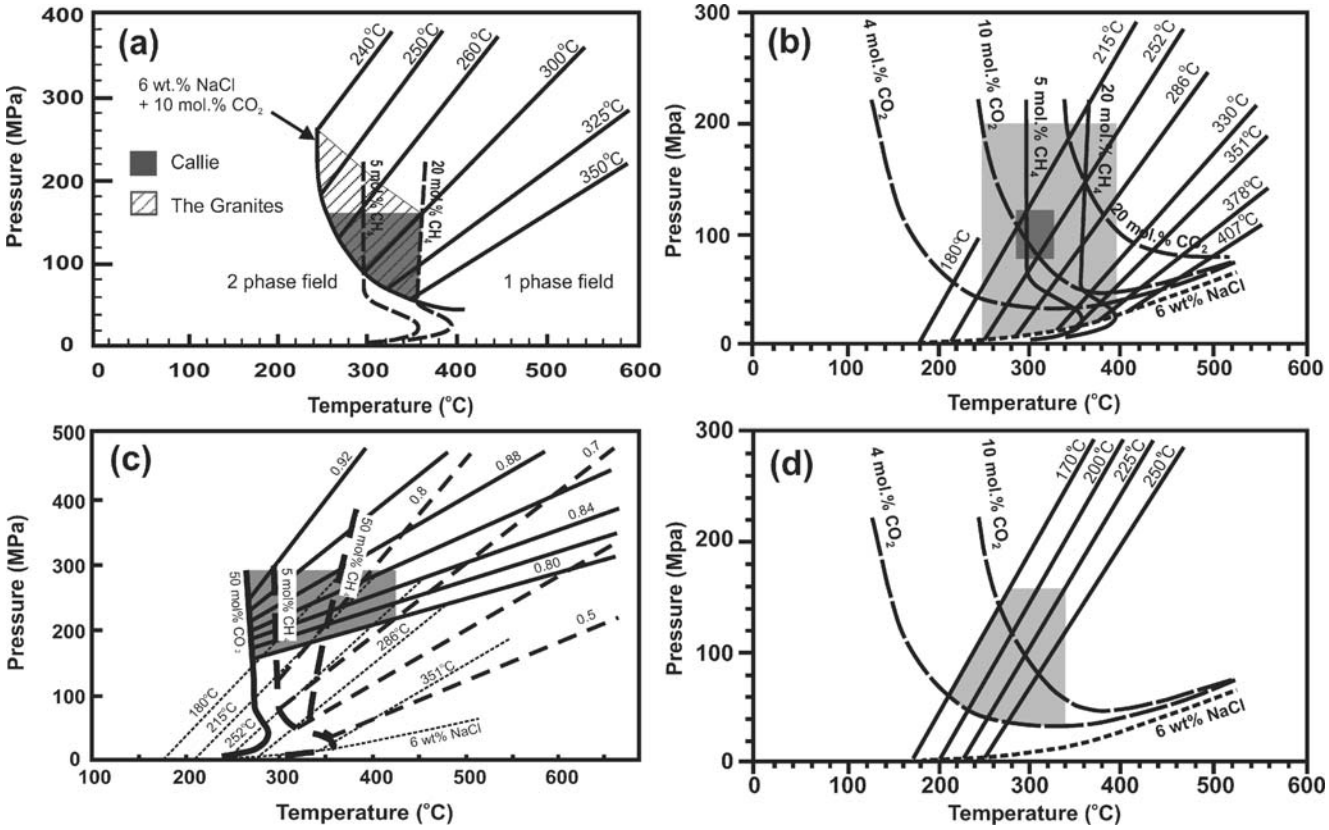

Fig. 11 Pressure vs temperature plots for **a** Callie (*gray region*) and The Granites goldfield (*hatched region*) showing the solvus for a 10-mol% CO_2+6 wt% NaCl solution (*thick solid line*) and lines of equal homogenization temperature (*thin solid lines*) from Schmidt and Bodnar (2000). The solvi for 5 and 20 mol% CH_4 in the system (CH_4+ H_2O) are shown by *thick dashed lines* (data from Duan et al. 1992). **b** The Coyote prospect showing the solvus for a 6-wt% NaCl solution (*short broken line*) and lines of equal homogenization temperature (*thin solid lines*). The solvi for 4, 10, and 20 mol% CO_2 in the system (CO_2 + H_2O + 6 wt% NaCl) are shown as *long broken lines* (data from Gehrig et al. 1986). The solvi for 5 and 20 mol% CH4 in the system (CH_4 + H_2O) are shown by *thick solid lines* (data from Duan et al. 1992). The *light gray region* represents the possible range of temperatures and pressures for Coyote, while the *dark gray box* represents the most probable conditions of trapping. **c** The Groundrush deposit (*gray region*) showing the solvi for 50 mol% CO_2 in the CO_2 + H_2O system and the 5-mol% CH_4 and 50-mol% CH_4 solvi for the CH_4–H_2O system. *Solid lines* show isochores of indicated density for the CO_2 + H_2O system. *Dashed lines* are isochores for the CH_4–H_2O system, and *broken lines* are for the H_2O–6 wt% NaCl system. **d** The Tanami goldfield (*gray region*) showing the solvus for a 6-wt% NaCl solution (*short broken line*) and lines of equal homogenization temperature (*thin solid lines*) from Schmidt and Bodnar (2000). The solvi for 4 and 10 mol% CO_2 in the system (CO_2+H_2O+6 wt% NaCl) are shown as *long dashed lines*

overlap of all deposits between 250 and 325°C. The fluids typically have low to moderate salinity but average salinities are generally higher than in most lode gold systems (Ridley and Diamond 2000), perhaps indicating a link to magmatic systems in this region (Mernagh et al. 2005). However, while the fluids have many similar characteristics, there is a notable change in the gas composition of the fluids with estimated depth of trapping. To understand how this may affect the mineralization processes, we will consider each deposit in terms of its estimated depth of formation.

Groundrush deposit

The Groundrush deposit occurs within dolerite that intrudes rocks of the Killi Killi Formation. This deposit appears to have formed at the greatest depth and records the highest mineralization temperatures. The quartz veins contain minor amounts of pyrite, pyrrhotite, and arsenopyrite but the wall rocks are relatively sulfide-poor with no visible alteration halo. This suggests that sulfidation of and fluid reaction with the host rock were not the main mechanism of gold deposition, thus requiring an alternative mechanism.

A feature of the ore-bearing fluids at Groundrush is their high CH_4 content. Similar CH_4-bearing fluids have also been reported from some Archean lode gold deposits (e.g., Mernagh and Witt 1994). Given the widespread occurrence of CO_2 fluids in lode gold systems, these methane-rich fluids could result from reduction of CO_2 by ferrous iron in silicates and oxide minerals in the surrounding mafic host rocks.

A possible mechanism for gold deposition is phase separation associated with pressure fluctuations associated with structural movement along faults and shear zones.

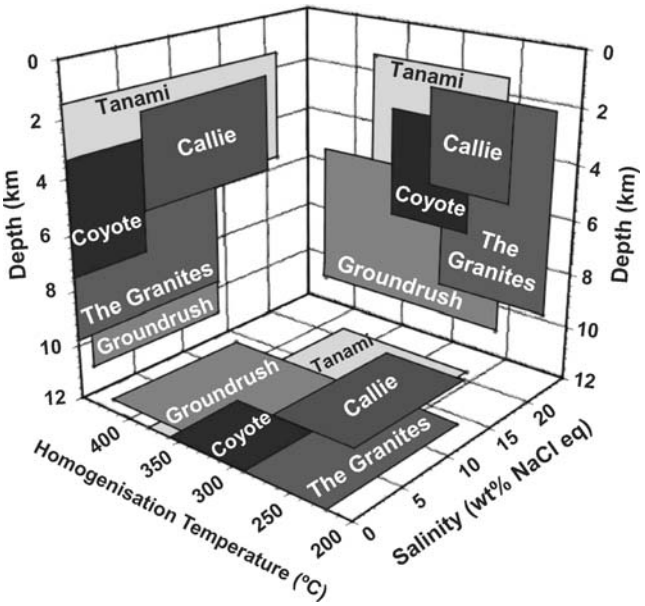

Fig. 12 A plot of total homogenization temperature, salinity, and estimated depths of trapping for fluid inclusions from the major ore deposits and prospects in the Tanami region

Sibson et al. (1988) have suggested that faults can act as valves, producing cyclical variations in fluid pressure from supralithostatic to hydrostatic. Gold is transported as a bisulfide complex and any hydrogen sulfide in the fluid will be strongly partitioned into the (CH_4+CO_2)-rich vapor phase.

Although this study found no direct evidence for phase separation, the process is not always recorded due to difficulties in trapping the vapor phase (Roedder 1984). Fluids, which contain CH_4, unmix over a wider range of pressures and temperatures than for the corresponding CO_2–H_2O system (Naden and Shepherd 1989), allowing phase separation and gold precipitation to occur at greater depths within the crust. Faulting and hydrofracturing may have led to pressure fluctuations, phase separation, and gold precipitation due to destabilization of the aqueous bisulfide complex. The dolerite host rocks may have facilitated this process given their relatively high competence.

The Granites goldfield

Deposits at The Granites goldfield are hosted by iron-rich sedimentary rocks of the Dead Bullock Formation and may have formed at depths approaching 10 km (Fig. 12). The fluids are dominated by CO_2 and N_2, with minor amounts of CH_4. Because the host rocks are iron-rich, it is likely some of the CH_4 in these fluids was generated by reaction with ferrous iron. Alternatively, the CH_4 may have been derived from the host rocks, which contain carbonaceous units. The fluid inclusion data provide evidence for phase separation, and thus, homogenization temperatures correspond to trapping temperatures. These trapping temperatures (240–312°C) are substantially lower than the estimation of metamorphic temperature based on mineral assemblages (600°C by Scrimgeour and Sandiford 1993). This suggests either that ore-stage quartz veins postdate metamorphism or that the fluid inclusions in the veins have reequilibrated at lower temperatures. The Granites goldfield is localized between two shear zones, which facilitated fluid flow and promoted interaction of the ore fluids with the iron-rich host units.

Narrow alteration zones around the veins contain pyrrhotite, pyrite, and arsenopyrite, which indicate that some gold precipitation resulted from desulfidation reactions. Desulfidation of the fluid is thought to occur through coupled reactions of the type:

$$'FeO'_{rock} + 2H_2S_{(g)} \leftrightarrow FeS_{2(py)} + H_2O + H_{2(g)} \quad (1)$$

and

$$Au(HS)_2^- + H^+ + 0.5H_{2(g)} \leftrightarrow Au + 2H_2S_{(g)} \quad (2)$$

However, as these alteration zones are narrow and given that there is good evidence for phase separation, it appears that initial precipitation of gold may have occurred by fluid–rock desulfidation reactions, but the main mechanism of gold precipitation was still desulfidation of the fluid during phase separation.

Coyote deposit

The fluids from the Coyote deposit differ from most of the other deposits in the Tanami region by the fact that there are three distinct fluid inclusion compositions (Fig. 9) and many fluid inclusions also contain graphite flakes. During prograde metamorphism of the sedimentary rocks, the composition of the fluids will depend on reactions between carbonaceous matter, carbonates, clays, and ferric iron minerals. At about 120°C, carbonaceous sedimentary rocks begin to lose CH_4 and graphite begins to form above 250°C (Holloway 1984). Between 250 and 350°C, graphite and vitrinite coexist and thus metamorphism of vitrinite provides a source of CH_4 to the fluid, while graphite is progressively forming.

However, as the graphite appears to be an accidentally trapped solid, it must have been present in the fluid before the formation of the fluid inclusions. Furthermore, since the trapping temperatures of the fluid inclusions are much lower than the activation energy of most graphite reactions (Ziegenbeim and Johannes 1980), little chemical interaction is expected between the fluid and graphite after trapping of the fluid inclusions. The presence of significant amounts of CO_2 in some graphite-containing inclusions also indicates

Table 4 Summary of the fluid compositions and alteration characteristics of the major ore deposits in the Tanami region

Goldfield	Ore fluid conditions	Fluid transport/ore controls	Vein assemblage/alteration	Depositional mechanism
Tanami (Mt. Charles Formation) 1.5–5.6 km	200–340°C 2–13 wt% NaCl eq. Rare occurrence of CO_2-rich fluids	Brittle faulting in basalt and sediments	Veins: qtz ± ser ± ank ± py ± chl ± sp ± aspy ± cpy Alteration: (1) ser+qtz+carb+py (inner zone) (2) chl+carb (outer zone)	Boiling/effervescence of a low salinity, CO_2-bearing fluid.
Callie (MacFarland Peak Group) 2.6–5.0 km	254–326°C 4–7 wt% NaCl eq. $CO_2 \pm N_2$	Sheeted quartz veins within a "structural corridor." Grade increases where there are high angle intersections between quartz veins and bedding planes. Increased porosity in zones of decarbonization.	Veins: originally qtz+feld(±biot ± epid) Alteration: (1) cc ± chl ± qtz ± py (upper levels) (2) chl ± tit ± ru (mid levels) (3) biot ± il ± epid ± po (lower levels)	(1) Reduction and /or effervescence of ore-bearing fluids from interaction with graphitic host rock (2) Zone refining to concentrate gold near the top of the decarbonised zone
Coyote (Killi Killi Formation) 3.4–7.5 km	290–360°C 0–7 wt% NaCl eq. (1) CO_2-rich ± graphite (2) CH_4-rich ± graphite (3) $CO_2 \pm N_2$	Brittle faulting in sediments	Veins: qtz ± py ± aspy ± cpy ± bism Alteration: qtz ± chl ± musc ± kaol	(1) Mixing of the ore-bearing fluids with more reduced fluids from carbonaceous sediments. (2) Boiling/effervescence of a low salinity, CO_2-bearing fluid.
The granites (Dead Bullock Formation) 3.0–9.8 km	240–312°C 0–14 wt% NaCl eq. $CO_2 \pm N_2 \pm CH_4$	Dilatant zones formed during folding in banded iron formation. Amphibolite grade host rocks adjacent to granite intrusions.	Veins: (1) qtz ± aspy ± po ± py (2) cc ± diop (3) qtz ± cc (4) clz ± qtz ± diop ± cc Alteration: (1) hbl(±cum ± epid ± chl) (2) diop ± clz ± hbl ± feld ± qtz (3) hbl ± diop ± clz ± feld ± qtz (4) hbl ± tit ± qtz ± feld ± il	(1) Desulfidation of ore fluids during boiling/effervescence (2) Reduction of the fluid by interaction with BIF host unit.
Groundrush (Killi Killi Formation) 5.6–11 km	260–430°C 1–14 wt% NaCl eq. $CH_4 \pm CO_2$	Quartz veining and brecciation in dolerite	Veins: qtz ± carb ± chl ± feld ± tit ± py ± po ± aspy ± cpy Alteration: chl ± carb ± act ± biot	Boiling/effervescence of a CH_4-rich fluid due to pressure fluctuations which lead to partitioning of H_2S into the vapor phase.

ser Sericite, *py* pyrite, *clz* clinozoisite, *qtz* quartz, *cpy* chalcopyrite, *cum* cummingtonite, *feld* feldspar, *sp* sphalerite, *diop* diopside, *carb* carbonate, *aspy* arsenopyrite, *po* pyrrhotite, *cc* calcite, *chl* chlorite, *lo* loelingite, *ank* ankerite, *hbl* hornblende, *tit* titanite, *musc* muscovite, *act* actinolite, *ru* rutile, *kaol* kaolinite, *epid* epidote, *il* ilmenite, *biot* biotite

that the fluids in these inclusions are not in equilibrium with graphite.

Similar to other deposits in the Tanami region, mineralization at Coyote is thought to be related to the D_5 deformational event and, hence, postdates earlier metamorphic events. The variable CO_2, N_2, and CH_4 concentrations in the fluids suggests that the ore-bearing fluids in the veins have mixed with fluids derived from the surrounding sedimentary rocks and particularly the carbonaceous units. The coexistence of aqueous fluid inclusions with both CO_2-bearing and CH_4-bearing inclusions indicates that phase separation also occurred as a result of pressure fluctuations during brittle deformation (Sibson et al. 1988). However, reduction of the ore-bearing fluids by fluid mixing is also an efficient method for precipitating gold and may be responsible for mineralization at the Coyote prospect. Therefore, both processes may have operated during mineralization at the Coyote prospect.

Callie deposit

The Callie deposit has similarities to the Coyote deposit, but is hosted by carbonaceous sedimentary rocks of the Callie Member. The fluid inclusion data indicate that Callie formed at similar or slightly shallower depths than Coyote (Table 4). At Callie, the ore-bearing fluid was enriched in CO_2 and N_2, but graphite is not observed in the fluid inclusions. This suggests that either there was less graphite in the rocks of the Callie Member, or more likely, that the larger volume of fluid flow at Callie completely consumed any graphite it came in contact with.

A multistage model has been developed the for mineralization at the Callie deposit (Wygralak and Mernagh 2001; Wygralak et al. 2005; Huston et al. 2007). In this model, oxidizing fluids reacted with carbonaceous sediments to reduce the fluid, decarbonize the host rocks, and produce CO_2. The concentration of CO_2 in the fluid increased until the fluid effervesced, which led to partitioning of H_2S into the vapor phase, and precipitation of gold by desulfidation of the fluid. Note that CO_2 effervescence only takes place at or near the decarbonization front. Furthermore, the amount of available carbonaceous material will have a direct impact on the amount of gold deposited. Consequently, more gold is predicted to precipitate in highly carbonaceous lithologies and structures containing the most carbon. Therefore, thickening of carbonaceous sedimentary rocks in fold hinges would enhance the effectiveness of gold deposition at these sites.

The post-ore, buck quartz veins contain Type D fluid inclusions with similar homogenization temperatures to those in the mineralized veins. The precipitation of chalcopyrite and galena in these veins indicates that the fluids were metal-bearing, but they lack any evidence of CO_2 or other gases typically associated with gold mineralization in this goldfield. The late post-mineralization (D_{6+}) ankerite and calcite veins contain fluids that have compositions similar to basinal brines and appear unrelated to the mineralization processes at Callie.

Tanami goldfield

The deposits that make up the Tanami goldfield appear to have formed at the highest crustal levels (Fig. 12 and Table 4) and many of the quartz veins have textures indicative of high-level emplacement. Therefore, these epizonal lode gold deposits have similarities to epithermal gold deposits. The rarity of CO_2-bearing inclusions is a common feature of epithermal systems (Cooke and Simmons 2000), as is partial fluid mixing (Field and Fifarek 1985). As stated above, the higher temperature, CO_2-rich fluid inclusions observed in the Southern and Jims Main pits are thought to represent the ore-bearing fluid before phase separation (i.e., loss of CO_2) and fluid mixing occurred. Significant loss of CO_2 from the fluid is to be expected from near surface, open systems at low pressure.

The majority of gold deposits in the Tanami goldfield are hosted by basalt, with the remainder hosted by turbiditic sedimentary rocks. As previously mentioned, the highest gold grades occur in dilatant zones and vein intersections, suggesting that boiling/effervescence due to pressure fluctuations was mainly responsible for gold precipitation. Fluid inclusions from the Tanami goldfield show the largest range of salinities (up to 21.2 wt% NaCl eq.). This range is much higher than that typically found in lode gold or epithermal systems (Ridley and Diamond 2000; Cooke and Simmons 2000). Therefore, the mixing trend shown in Fig. 7 may indicate mixing of the lower salinity CO_2-bearing fluid with the high salinity pre-ore fluid or, more probably, mixing with the high salinity post-ore fluid reported by Tunks (1996) and Tunks and Cooke (2007).

Conclusions

Fluid inclusion studies indicate that trapping temperatures of the ore-bearing fluids in the Tanami region range from 200 to 430°C, but there is a general overlap of temperatures between 250 and 325°C (Fig. 12) for all the deposits considered in this study. Pressure estimates indicate that the gold deposits formed over a range of depths (Table 4), with Groundrush forming at the greatest depth (5.6–11 km) and the Tanami goldfield forming at the highest crustal levels (1.5–5.6 km). Laser Raman spectroscopic studies also show a variation in gas ratios, with greater amounts of CH_4 in the deeper, higher temperature deposits (e.g., Groundrush), and a higher proportion of $CO_2 \pm N_2$ in

higher-level deposits (e.g., Callie). CH_4 is probably derived from the interaction of the fluid with either mafic or sedimentary lithologies, but the gas ratios are ultimately controlled by the oxidation state of the fluid. The stable isotope data indicate either a magmatic or mixed magmatic/metamorphic source for the ore fluids in the Tanami region with some minor mixing with meteoric fluids.

Mineralization is related to brittle fractures and other dilational structures, but in the larger deposits, there is also an association with iron-rich rocks or carbonaceous sediments, suggesting that both structural and chemical controls are important. The fluid inclusion data indicate that the major mineralization process was boiling/effervescence of a gas-rich fluid, which led to partitioning of H_2S into the vapor phase and gold precipitation. However, some deposits also show evidence of desulfidation by fluid–rock interaction and/or reduction of the ore-fluid by fluid mixing. Therefore, the Paleoproterozoic gold deposits in the Tanami region appear to conform to the continuum model for lode gold deposits suggested by Groves (1993) for Archean districts. The presence of CH_4 in the fluid will enhance phase separation in the deeper deposits, while pressure fluctuations at higher crustal levels leads to phase separation that may also be accompanied by greater fluid–rock interaction and fluid mixing.

Acknowledgements The authors wish to thank Newmont Australia Ltd., Tanami Gold, and Anglogold Australasia Ltd, for access to their deposits and drillcore and for assistance while in the field. We are especially grateful to Susan Golding (University of Queensland) for the hydrogen, oxygen, and carbon isotopic analysis. Richard Goldfarb, Philip Brown, Larryn Diamond, David Huston and Subhash Jaireth are thanked for constructive suggestions and comments on earlier drafts of this manuscript. TPM publishes with the permission of the Chief Executive Officer of Geoscience Australia.

Appendix

Table 5 Deposit location and description of samples collected for fluid inclusion analysis

Sample number	Deposit/Pit	Description and comments
Callie Deposit		
Pre-ore veins		
11665	Callie	DBD412, early, pre-ore folded quartz vein
11670	Callie	DBD412, folded pre-ore vein
11357	Callie	Pre-ore quartz vein cut by 11356
11454	Callie	Pre-mineralization deformed quartz vein from RL 1020
11457	Callie	Pre-min. quartz vein 25/30 W from RL 1020
11460	Callie	Pre-min. quartz vein 0/45E from RL
Ore-bearing Veins		
11222	Callie	Auriferous discordant quartz vein from 1120RL
11336	Callie	Hole GBD 117, ore stage quartz vein, same as 11222
11349	Callie	Hole GBD 268, Blake beds
11355	Callie	Ore stage quartz vein 60/65S from RL 1120
11356	Callie	Ore stage quartz vein 75/70S from RL 1120
11358	Callie	Ore stage quartz vein 65/60S from RL 1080
11359	Callie	Ore stage quartz vein 65/60S from RL 1080
11360	Callie	Ore stage quartz vein 55/60S from RL 1020
11361	Callie	Ore stage quartz vein 70/50SE from RL 1020
11362	Callie	Ore stage (visible Au) quartz vein 65/55S from RL 980
11363	Callie	Ore stage (visible Au) quartz vein 65/70S from RL 980
11455	Callie	Syn-min. W dip, quartz vein (pair with 11454) from RL 1020
11456	Callie	Syn-min. quartz vein 170/30E from RL 1020
11459	Callie	Tension gashes in basic intrusive from RL 990
11461	Callie	Syn-min. quartz vein 70/70 from RL 830
Post-ore veins		
11223	Callie	Late carbonate vein cutting 11222
11674	Callie	DBD410D2, post-ore quartz–carbonate vein with sphalerite, galena and sericitic selvage
11416	Callie	Hole DBD 300, very clean calcite
11417	Callie	Hole DBD 300, vein of post-ore "buck" quartz
11418	Callie	Hole DBD 268, vein of post-ore "buck" quartz
11447	Callie	Pre-mineralization quartz vein 60/15S from RL 1060
11448	Callie	Post-mineralization quartz vein 170/20Efrom RL 1060
11449	Callie	Post-mineralization quartz vein 45/45SE from RL 1060
11450	Callie	Post-min. quartz–carbonate vein 170/45E from RL 1020
11451	Callie	Post-mineralization quarttz vein 35/30S from RL 1020
11458	Callie	Post-min. quartz vein 50/70SE from RL 1020
The Granites Goldfield		
Ore-bearing veins		

Table 5 (continued)

Sample number	Deposit/Pit	Description and comments
11210	West Bullakitchie	Hole GBD 203, quartz vein in schist;
11211	West Bullakitchie	Hole GBD 203, quartz vein in carbonate; host: schist with garnets
11212	West Bullakitche	Hole GBD 203, quartz vein in schist with no garnets
11214	East Bullakitchie	Hole GBD 58, ore zone
11215	East Bullakitchie	Hole GBD 58
11217	East Bullakitchie	Hole GBD 58
11220	East Bullakitchie	Hole GBD 58
11243	Shoe	Hole SEX 004, quartz vein of uncertain orientation
11244	Shoe	Hole SEX 004, quartz vein of uncertain orientation
11253	Quorn	Hole GQD 219, ore zone
11262	Quorn	Hole GQD 219, hangingwall(?)
11263	Quorn	Hole GQD 219, footwall(?)
11334	East Bullakitchie	Hole GBD 117, schistosity parallel quartz vein
11335	East Bullakitchie	Hole GBD 117, calc-silicate vein with sulfides
11854	Quorn	Quartz-pink spar vein in Inningarra (?) granite; pink K-feldspar
11855	Quorn	Quartz vein in Inningarra granite
11856	Quorn	Quartz vein in Inningarra granite
Coyote Prospect		
Ore-bearing veins		
11545	Coyote	CYDD9, quartz vein in siltstone, assay 1400 g/t Au
11546	Coyote	CYDD9, quartz vein in siltstone, assay 8 g/t Au
11780	Coyote	CYD0016, 200.5 m, native Au
11781	Coyote	CYD0016, 205.3 m
11783	Coyote	CYDD24, 243.5 m, native Au
11784	Coyote	CYD24, 242.5 m, native Au, 354 g/t Au
11785	Coyote	CYD24, 239.5 m, 65.0 g/t Au
11789	Coyote	CYDD14, 197.2 m
11791	Coyote	CYDD13, 183.6 m, ~6 g/t Au
Groundrush Deposit		
Ore-bearing Veins		
11519	Groundrush	No grade, late epithermal quartz vein
11520	Groundrush	Groundrush dolerite
11521	Groundrush	High-grade ore (16.5 g/t Au), quartz vein in dolerite with a speck of visible gold on the contact
11524	Groundrush	Ore zone, brecciated quartz veins, speck of gold on styllolite
11526	Groundrush	Ore zone, speck of gold in quartz vein
Tanami Goldfield		
Pre-ore veins		
10991	Carbine	"Triple point" early quartz in basalt

Table 5 (continued)

Sample number	Deposit/Pit	Description and comments
11018	Southern	Quartz vein 180/30 W in basalt;
11056	Carbine	Hole CAD 57, vein of white clean quartz in basalt
11061	Carbine	Quartz pot in basalt but not a triple point
11064	Southern	Quartz vein 25/65E
Ore-bearing veins		
10990	Carbine	Basalt hosted quartz vein 190/45 W in the ore zone
10994	Dogbolter	Brecciated white quartz from the ore zone
10995	Dogbolter	Pegmatite-like quartz–white feldspar vein, 140/90
11005	Hurricane	Felsic dyke 80/70S
11006	Hurricane	Silicified shear 40/90
11007	Hurricane	Hole HRD 001. Cross cutting relations between veins
11008	Hurricane	Hole HRD 001. Cross cutting veins; just slide
11009	Hurricane	Hole HRD 001. 10 cm thick vein of white quartz with sulfide
11010	Hurricane	Hole HRD 001. Quartz–carbonate vein with sulfides.
11012	Hurricane	Hole HRD 20. Quartz–carbonate vein next to previous sample
11016	Carbine	Hole CAD 14. Quartz vein with pink feldspar in altered basalt
11020	Southern	Quartz vein 45/75SE
11021	Southern	Quartz vein 40/65SE
11022	Miracle	Lens of white quartz in basalt
11023	Miracle	Jasper-like quartz (hot spring?)
11024	Dinky	Lens of white, laminated, vuggy quartz in basalt
11025	Dinky	"Dog teeth" quartz vein 15/35E. Late quartz or low temperature vein?
11027a	Dinky	Bedding parallel quartz vein with jasper. Sample of quartz
11027b	Dinky	Same vein as above. Sample of jasper
11029	Southern	Ore zone. Quartz vein 30/35SE
11031	Carbine	Quartz vein from the ore zone
11032	Carbine	Pod of quartz in basalt. Ore zone
11036	Carbine	Vein of "sugary" quartz
11037	Bouncer	Basalt hosted brecciated tension gash(?) vein of white quartz; 20/45NW
11038	Bouncer	Quartz vein 140/75SW in basalt. Ore zone
11039	Bumper	Quartz vein 20/75 W
11041	Carbine	White, cavernous quartz vein. 50/65NW. Ore stage
11042	Carbine	Hole CAD 14, 15 cm thick carbonate–K–feldspar (?) vein with pyrite
11046	Carbine	Hole CAD 15, quartz vein next to 11045
11049	Carbine	Hole CAD 15, ore zone, brecciated quartz
11053	Carbine	Hole CAD 009, brecc. quartz with

Table 5 (continued)

Sample number	Deposit/Pit	Description and comments
		carbonate veinlets and pyrite, ore zone, 5.5 g/tAu
11057	Legs	Concordant vein of white quartz 25/35 W, visible Au
11058	Legs	Lensoidal veins of cavernous quartz with white clay, 25/30 W, ore stage
11059	Legs	Shear parallel quartz vein 5/70E
11060	Legs	Concordant vein of cavernous quartz 160/60NE
11063	Bouncer	Quartz vein 30/30E, ore stage
11065	Hurricane	Quartz stockwork 145/75NE in Hurricane Sediment, ore stage(?) quartz
11066	Hurricane	Quartz vein 35/vert.; similar to 10006
11067	Hurricane	Quartz vein 60/45NW
11068	Hurricane	Quartz boulder with malachite, stage V (post-ore)
11069	Carbine	Hole CAD 1, gray basalt with chloritic(?) black spots
11070	Carbine	Hole CAD 1, unaltered basalt
11073	Carbine	Hole CAD 1, ore z. 15.1 g/tAu, carbonate vein with py, stage IVa
11079	Legs	Hole RDH 23, ore z. 3.77 g/tAu, quartz–carbonate vein
11088	Phoenix	Quartz vein 30/65E
11089	Phoenix	Quartz vein 130/vert.; ore stage?
11090	Phoenix	"Ponytailing" quartz vein 20/80E, ore stage?
11091	Bastille	Cavernous quartz with white clay, ore z. 9 g/tAu
11092	Bastille	Pods of quartz with "karsted" surface
11096	Money	Brecciated quartz in shear 60/70SE, ore zone
11097	Money	Brecciated quartz in shear 60/70SE, ore zone
11100	Redback SE	Ore stage quartz vein 45/60SE
11101	Redback SE	Post-ore quartz vein
11112	Dogbolter	Hole DDH 029, rich (130 g/t) mineralised zone with native Au and pyrrhotite in chloritized quartz–carbonate veinlets
11117	Dogbolter	Hole DDH 042, rich miner. (46.35 g/tAu), "jigsaw" breccia of gray quartz, Au, pyrite, pyrr, carbonate
11118	Dogbolter	Hole DDH 042, (130 g/tAu) in quartz
11123	Jim's Main	Ore stage (IVA) quartz vein 10/55 W
11125	Jim's Main	Ore stage (IVA) quartz vein 110/45NE
11130	Jim's Main	Hole JDH 006, carbonate vein
11132	Jim's Main	Hole JDH 022, high grade (108.5 g/tAu) ore zone
11137	Banjo	Hole PDGH 011, quartz vein in brecciated sltst. ore zone >10 g/tAu
11140	Beaver Creek	Hole PDH 009, brecciated quartz–carbonate vein
11141	Beaver Creek	Hole PDGH 009, ore z. 0.8–18 g/tAu, brecc.quartz–carbonate veins
11142	Beaver Creek	Hole PDGH 009, ore z. 0.8 g/tAu, well-defined quartz vein
11147	Harleys	Sedim. hosted vein of chalcedonic quartz 160/70 W
11148	Huntswoman	Quartz vein 60/55SE with boxwork textures
11149	Huntswoman	Quartz vein 35/50E in shear (ore stage quartz)
11150	Daddys South	Ore stage quartz vein 50/60SE

References

Adams GJ (1997) Structural evolution and ore genesis of The Granites gold deposits, Northern Territory. B.Sc.(Hons) Thesis, University of Adelaide. Adelaide, Australia, 210pp

Bagas L, Huston D, Anderson J (2007) Gold deposits in the Palaeoproterozoic Tanami Group, Western Australia. Miner Deposita (in this issue)

Bakker RJ (1997) Clathrates: Computer programs to calculate fluid inclusion V–X properties using clathrate melting temperatures. Comput Geosci 23:1–18

Bodnar RJ, Vityk MO (1994) Applications of fluid inclusions in tectonic reconstruction: microthermometric analysis. In: Izquierdo MG, Suarez AMC, Guevara GM, Vanko D, Viggiano GJC (eds) Fifth biennial Pan-American conference on research on fluid inclusions, Cuernavaca, Mexico, 19–21 May 1994, p 10

Brincat J (1994) The vein paragenesis and mineralization of the East Bullakitchie mine, The Granites goldfield, Northern Territory. University of Adelaide, Australia, 35pp

Brown PE, Hagemann SG (1995) MacFlinCor and its application to fluids in Archaean lode–gold deposits. Geochim Cosmochim Acta 59:3943–3952

Clayton RN, Mayeda TK (1963) The use of bromine pentafluoride in the extraction of oxygen from oxides and silicates for isotopic analysis. Geochim Cosmochim Acta 27:43–52

Clayton RN, O'Neil JR, Mayeda TK (1972) Oxygen isotope exchange between quartz and water. J Geophys Res 77:3057–3067

Clayton RN, Golodsmith JR, Mayeda TK (1989) Oxygen isotope fractionation in quartz, albite, anorthite and calcite. Geochim Cosmochim Acta 53:725–733

Cooke DR, Simmons SF (2000) Characteristics and genesis of ephemeral gold deposits. In: Hagemann SG, Brown PE (eds) Gold in 2000. Reviews in Economic Geology, vol. 13. Society of Economic Geologists, pp 221–244

Crispe AJ, Vandenberg LC, Scrimgeour IR (2007) Geological framework of the paleoproterozoic Tanami region, Northern Territory. Miner Deposita (in this issue)

Duan Z, Moller N, Weare JH (1992) An equation of state for the CH_4–CO_2–H_2O system: II Mixtures from 50 to 1000 C and 0 to 1000 bar. Geochim Cosmochim Acta 56:2619–2631

Duan Z, Moller N, Weare JH (1996) A general equation of state for supercritical fluid mixtures and molecular dynamics simulation of mixture PVTX properties. Geochim Cosmochim Acta 1209–1216

Dubessy J, Audeoud D, Wilkins R, Kosztolanyi C (1982) The use of the Raman microprobe MOLE in the determination of the electrolytes dissolved in the aqueous phase of fluid inclusions. Chem Geol 37:137–150

Field CW, Fifarek RH (1985) Light stable-isotope systematics in the epithermal environment. In: Berger BR, Bethke PM (eds) Geology and geochemistry of epithermal systems. Reviews in Economic Geology, vol. 2. Society of Economic Geologists, pp 99–128

Friedman I (1953) Deuterium content of natural waters and other substances. Geochim Cosmochim Acta 4:89–103

Gehrig M, Lentz H, Franck EU (1986) The system water–carbon dioxide–sodium chloride to 773 K and 300 MPa. Ber Bunsenges Phys Chem 90:525–533

Groves DI (1993) The crustal continuum model for late-Archaean lode gold deposits of the Yilgarn block, Western Australia. Miner Depos 28:366–374

Guoyi D (1994) A progress report of fluid inclusion and petrology from the Callie deposit, The Granites, NT. North Flinders Exploration Ltd. Internal Report

Higgins NC (1990) Moderately depleted oxygen isotope composition of waters associated with tin- and tungsten-bearing quartz veins: an evaluation of isotopic models. In: Herbert HK, Ho SE (eds) Stable isotopes and fluid processes in mineralization, vol. 23. University of Western Australia, pp204–214

Hoefs J (1980) Stable isotope geochemistry. Springer, Berlin Heidelberg New York, 208pp

Holloway JR (1984) Graphite–CH_4–H_2O–CO_2 equilibria at low-grade metamorphic conditions. Geology 12:455–458

Huston DL, Wygralak AS, Mernagh TP, Vandenberg LC, Crispe AJ, Lambeck L, Cross A, Fraser GL, Williams NC, Worden K, Meixner A (2007) Lode gold mineral system(s) of the Tanami Region, northern Australia. Miner Deposita (in this issue)

Mernagh TP, Witt WK (1994) Early, methane-rich fluids and their role in Archaean gold mineralization at the Sand King and Missouri deposits, Eastern Goldfields Province, Western Australia. AGSO J Aust Geol Geophys 15:297–312

Mernagh TP, Bastrakov EN, Wyborn LAI (2005) A comparison of some chemical processes of ore precipitation in orogenic and intrusion-related gold mineral systems. structure, tectonics and ore mineralisation processes (STOMP). Abstracts Volume, EGRU Contribution No. 64, p.89

Morrison G, Guoyi D, England D (1994) A reconnaissance of alteration and mineralisation petrology and fluid inclusions from the Callie deposit, The Granites, NT. North Flinders Exploration Ltd. Internal Report

Naden J, Shepherd TJ (1989) Role of methane and carbon dioxide in gold deposition. Nature 342:793–795

Ridley JR, Diamond LW (2000) Fluid chemistry of orogenic lode gold deposits and implications for genetic models. In: Hagemann SG, Brown PE (eds) Gold in 2000. Reviews in Economic Geology, vol. 13. Society of Economic Geologists, pp 141–162

Roedder E (1984) Fluid inclusions. In: Ribbe PH (ed) Reviews in mineralogy, vol.12. Mineralogical Society of America, 644pp

Schmidt C, Bodnar RJ (2000) Synthetic fluid inclusions: XVI. PVTX properties in the system H_2O–NaCl–CO_2 at elevated temperatures, pressures, and salinities. Geochim Cosmochim Acta 64:3853–3869

Scrimgeour I, Sandiford M (1993) Early Proterozoic metamorphism at the Granites gold mine, Northern Territory: implications for the timing of fluid production in high-temperature, low-pressure terranes. Econ Geol 88:1099–1113

Sibson RH, Robert F, Poulson KH (1988) High-angle reverse faults, fluid pressure cycling and mesothermal gold–quartz deposits. Geology 16:551–555

Smith JB (2000) NTGS-AGSO Geochronology Project Report 3. Australian Geological Survey Organisation Professional Opinion 2000/27. Australian Geological Survey, Canberra, Australia

Smith MEH, Lovett DR, Pring PI, Sando BG (1998) Dead Bullock Soak gold deposits. In: Berkman DA, Mackenzie DH (eds) Geology of Australian and Papua New Guinean mineral deposits, The Australasian Institute of Mining and Metallurgy, Melbourne, pp 449–460

Tanami Gold NL (2003) Coyote gold project, media release. 23 December 2003, 6pp

Tanami Gold NL (2005) High grade resource increase at Coyote. Quarterly report, 7 February 2005, 4pp

Taylor BE (1987) Stable isotope geochemistry of ore-forming fluids. In: Kyser TK (ed) Short course in stable isotope geochemistry of low temperature fluids, vol. 13. Mineralogical Association of Canada, pp 337–452

Thomas AV, Spooner ETC (1988) Fluid inclusions in the system H_2O–CH_4–NaCl–CO_2 from metasomatic tourmaline within the border unit of the Tanco zoned granitic pegmatite. Geochim Cosmochim Acta 52:1065–1075

Tunks AJ (1996) Geology of the Tanami Gold Mine, Northern Territory. Ph.D. Thesis, University of Tasmania, Hobart, Australia, 239pp

Tunks AJ, Cooke DR (2007) Geological and structural controls on mineralization of the Tanami gold mine. Miner Deposita (in this issue)

Vandenberg LC, Hendrickx MA, Crispe AJ, Slater KR, Dean AA (2001) Structural geology of the Tanami Region. Northern Territory Geological Survey, Record 2001–004, 20 pp

Williams NC (2007) Controls on mineralisation at the world-class Callie gold deposit, Tanami desert, Northern Territory, Australia. Miner Deposita (in this issue)

Wopenka B, Pasteris JD (1987) Raman intensities and detection limits of geochemically relevant gas mixtures for a laser Raman microprobe. Anal Chem 59:2165–2170

Wygralak AS, Mernagh TP (2001) Gold mineralization of the Tanami region. Northern Territory Geological Survey, Record 2001–011, 40 pp

Wygralak AS, Mernagh TP, Huston DL, Ahmad M (2005) Mineral gold system of the Tanami region. Northern Territory Geological Survey, Report 2004-18

Ziegenbeim D, Johannes W (1980) Graphite in C–H–O fluids: an unsuitable compound to buffer fluid composition at temperatures up to 700C. Neues Jahrb Mineral Abh 7:289–305